Mining, Metallurgy & Exploration (2022) 39:2095–2120
https://doi.org/10.1007/s42461-022-00650-9

Predicting and Optimising the Strength of Cemented Paste Fills Through Bayesian Network Model

Kanhaiya Mishra[1] · P. S. Paul[2] · C. N. Ghosh[1] · Prashant Singh[1] · S. K. Behera[1] · Phanil. K. Mandal[1]

Received: 27 August 2020 / Accepted: 29 June 2022 / Published online: 14 July 2022

Abstract
The techno-economic and social benefits of cemented paste backfill (CPB) resulted in its wide acceptance by the mining industry. The Ordinary Portland Cement (OPC) remains the key binder but to diminish its economical constraints, suitability of alternate binders has been examined worldwide. The present study aimed to investigate the effect of partial replacement of OPC with fly ash on the CPB's strength and to determine the most optimal mix to achieve the required strength (1 MPa at 28 days of curing) at the most cost-effective way using the Bayesian network (BN). The CPB mixes were prepared at 72 wt.% solid concentration with mill tailings (87–91%), OPC (6–13%), and fly ash (0–4%), and instantly after mixing, fresh (slump, bleeding, density) CPB properties were measured. The strength was tested at 7, 14, 28, and 56 days of curing and initially analysed through traditional model. The traditional models follow the aleatory principle and are considered not appropriate for geotechnical engineering. Hence, the BN model was developed and tested. The reliability of two classifiers in learning model structure was compared which gives Naïve Bayes as the highest reliable tool. The CPB's strength is most sensitive to the OPC content. The most consistent mix(s) is mill tailings: 87–88%, OPC: 9–11%, fly ash: 1–4%. Adding fly ash at 89–91wt% mill tailings possesses high failure probability of the CPB. The collinearity test indicates that the fines percentage and chemical composition of CPB's ingredients are highly correlated with its slump, bleeding, and strength development.

Keywords CPB structure · Fly ash · UCS · Uncertainty · Bayesian network model · Failure probability

1 Introduction

The mining industries have witnessed numerous technological advancements in various domains during the past few decades [1–5]. The cemented paste backfilling (CPB) system is one paradigm which is gradually adopted by many countries as an alternate to the conventional backfilling techniques [6–10]. In comparison to the hydraulic backfill, paste augments the utilization of total tailings, reduces mine cycle times due to quick confinement, lessens water consumption and bleeding, and increases ore recovery [11–15]. Paste fills are prepared with the mill tailings, a binding material (such as cement, fly ash, lime, limestone powder, granulated blast furnace slag, granulated marble waste, jarosite, volcanic tuff, and pumice), and some water added to attain the requisite rheological and strength characteristics as shown in Fig. 1 [16–19]. In general, a grainy substance must be at least 15% finer than 20 µm to form a paste (non-settling slurry) with the desired flow properties. The bleeding of water through paste fills is very minimal, to practically no water bleed.

The mechanical properties of the CPB must endure the loads imposed during the adjoining mining activities [20]. Indeed, the mine backfill failures have substantial economic consequences and often result in fatalities or injuries [21]. The prevalent mechanical parameter that governs the stability criterion of the CPB is the unconfined compressive strength (UCS) [22–25]. The most likely reason is that the UCS test is rather quick and cost effective, and mines can easily adopt it in routine practice [26, 27]. The binding dosage particularly Ordinary Portland Cement (OPC) significantly augments the cohesion and strength of the paste fills to enable ground support installation requirements [28–32]. The desired strength of the backfilled mass is a site-specific constraint and based upon that value, the binder proportions are adjusted. The target strength values of the CPB

✉ P. S. Paul
partha_sp99@yahoo.com

[1] Mine Backfilling Department, CSIR- Central Institute of Mining and Fuel Research, Dhanbad 826001, India

[2] Department of Mining Engineering, IIT (Indian School of Mines), Dhanbad 826004, India

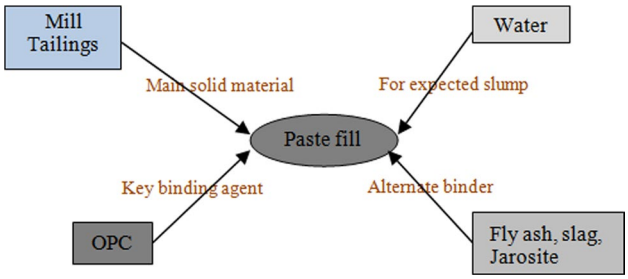

Fig. 1 Constituents of paste fills

Table 1 Strength requirement for CPB structure in different circumstances

Reference	Purpose	Target strength
Landriault[33]	Filling of voids	150–300 kPa
Grice[34]	Roof support	≥4 MPa
Yumlu[35]	Self-supporting stopes	1 MPa
Been et al.[36], Roux et al.[37]	To prevent the liquefaction risk	0.15 MPa

for different functions as reported in past studies are summarised in Table 1.

Previous studies have pointed out that the CPB operation consumes nearly 10–20% of the overall cost of the mining operation [34]. The volume of the binder can exhibit up to 75% cost of the CPB's operation [38]. Therefore, it is rather imperious to optimise the binder type and dosage to minimise the cost of the CPB. In this regard, the partial replacement of the OPC with different pozzolanic materials, such as fly ash, silica fume, slag, jarosite, and pumice, has been found to reduce the binder cost for desired strength [30, 39–44]. Likewise, the targeted strength of the paste fills can be acquired cost-effectively by increasing solid proportion rather than augmenting binder dosage [8].

The past attempts to access the stability of the paste backfill structure in underground stopes are summarised in Table 2. Different approaches were taken up by the researchers such as (i) numerical approach, to set the critical strength requirement in different stope conditions, study of arching effect and stress–strain relationship, etc.; (ii) analytical approach, to predict the CPB's strength with different mix configurations and to calculate the target strength for specific sites; (iii) laboratory experiments, to find out the most suitable mix configuration to achieve the targeted strength; and, finally (iv) field trials, for monitoring the quality of backfill and to optimise the system design. These studies have clearly demonstrated that the strength development of the paste fills depends on the solid percentage and characteristics of the ingredients. The binder hydration and growth of the cement gel along with the curing age reduce the permeability and void ratio of the CPB matrix and result in solid skeleton mass of higher strength. The hydration of the binding agents as well as precipitation of the hydrated phases causes hardening of the paste backfill [30]. Few researchers have also observed that the presence of sulphide minerals as well as soluble sulphates causes deterioration of the strength of the paste backfill due to sulphate attack [45–47].

The strength development within the paste fills is the coupled interaction mechanism and specific to the materials' characteristics. The previous studies as shown in Table 2 have well explained the strength growth mechanism of the CPB for different kinds of materials. These studies were primarily focussed on the histogram plot of the experimental characteristics of the CPB which may not capture the complexity, nonlinearity, and uncertainties in the datasets. The research community have paid very limited attention to the strength development of CPB under the coupled interaction effect of the influencing variables. Few authors have presented the advanced mathematical computation tools such as artificial neural network (ANN), multiple regression modelling, particle swarm optimisation, regression tree for prediction of the strength, and optimisation of the mix ratio of the paste fills [26, 32, 54–57, 67–71]. These models originated from the traditional statistics and therefore have some drawbacks as explained below:

- The conventional models coalesce the variance within whole datasets and provide one single and fixed parameter as a consequence. Geotechnical datasets show continuous variation; hence, it may be better to represent the parameter in the form of probability density function.
- These models are very specific to the materials' characteristics and the number of predictors.
- The traditional models could not capture the uncertainties associated within the multidimensional datasets.
- These models do not consider the categorical influence of the input variables on each other.

To overcome these limitations, a model is required which could capture the uncertainties within the datasets, prioritise the variables based on their relative significance, and have a high generalisation capability. The study of Permai and Tanty [72] revealed that the reliability of the Frequentist models is not as much of those models developed at the Bayesian platform. The Frequentist statistics deals with the "aleatory uncertainties" which arise due to the random behaviour of the system [73], whereas Bayesian statistics is suitable in case we have incomplete information of the system and thus fall under the "epistemic uncertainty". Uncertainty which associated with the every design aspect of engineering is probably due to "epistemic uncertainty" that resulted from the case-specific variation in the datasets and data scarcity and can be reduced by the knowledge updating

Table 2 Previous studies to access the stability of paste backfill

Reference	Type of study	Purpose	Outcome
Helinski et al.[6],Yilmaz[9, 47–53]	Numerical approach	To set the system design requirement	Stope conditions were simulated to determine stress–strain relationship and the stability of backfilled mass
Behera et al.[32],Fall and Benzaazoua[38, 54–57]	Analytical approach	To predict and optimise the strength vis-à-vis mix design	Authors developed models to predict the strength as well as to optimise the binder dosage for critical strength limit
Ghirian and Fall[7],Singh et al.[19],Fall and Benzaazoua[22],Fall and Pokharel[26],Yilmaz et al.[29],Benzaazoua et al.[30],Behera et al.[32, 58–62]	Laboratory experiments	To meet the design criteria and to find out the most suitable mix recipes	Cylindrical specimens were prepared and cured in an atmospheric condition or in a humidity chamber before testing for strength. Strengths were found to vary with binder type/dosage and solid %age
Chen et al.[27, 63–66]	Field experiments	Monitoring of designed criteria for quality control and to enhance the performance of the system	The paste fills were subjected to shearing during flow through pipelines. In situ cores were taken for strength testing. Strength was found to be different from lab results and varies along and across the stope

[74, 75]. In the geo-technical and its linked fields, these conditions most often arise when it becomes essential to make predictions with limited datasets or continuous variations in the datasets. The Bayesian network (BN) model, which works on the principle of the Bayes theorem of conditional probability distribution, naturally deals with the uncertain dependency among the variables and helps in building useful predictions, classifications, and belief updating [76]. The efficacy of the BNs has been explored in various domains of the geo-technical engineering to establish the dependency relationship between the causal factors and prioritisation of the factors based on their relative significance, as well as determining the range of datasets having the least level of uncertainty [77–81]. However, rarely has any study addressed the effectiveness of the BNs in modelling paste fill strength.

The present study undertakes the investigation for evaluating the strength of paste fill mix with different proportions of mill tailings and OPC. For cost-saving purposes, additional investigations were performed by partially substituting the OPC with the same weight fraction of fly ash with the maximum replacement level up to 4%. Primarily, the experimental datasets have been presented through the conventional plot. In order to establish the complicated and nonlinear constitutive dependency among the CPB's strength predictors, the BN was developed with different classifier structures. Primarily, the reliability of these classifiers towards building the model structure was compared and the model with the highest consistent classifier was selected for subsequent analysis. The BN model was then used to compute the comparative significance of the influencing factors towards the strength growth. Furthermore, the potential of the CPB specimens of different mix proportions to attain the desired strength at a specified curing age was estimated. Therefore, the optimum mix proportion having the least level of uncertainty and the highest estimated strength was determined. The Netica Software developed by Norsys Software Corporation was used for BN modelling in this study [82].

2 Materials and Methods

The study was conducted for one of the lead–zinc mines situated in the western part of India. The mine is operating with the blast hole stoping along with cemented paste backfilling. The mill tailings (lead–zinc waste material) are used as a main backfill material and Ordinary Portland Cement (OPC) as a sole binding agent for preparing paste fills at 72% solid weight concentration to achieve the targeted strength 1 MPa at 28 days of curing. This requisite strength was estimated by the analytical solution proposed by Mitchell et al. [83] and Li and Aubertin [84], and numerical modelling technique, by considering the general stope block dimension

Table 3 Particle size distribution of previously reported mill tailings

Reference	Tailings type	G_S	D_{10}	D_{30}	D_{50}	D_{60}	D_{90}
Ghirian and Fall[7]	Zinc	3.34	1.6	10.9	29.9	37.8	-
Ghirian and Fall[7]	Silica	2.7	1.9	9.0	22.5	31.5	-
Célestin and Fall[21]	Silica	-	1.9	9.0	22.5	31.5	88.9
Fall and Pokharel[26]	Silica	2.7	1.9	9.0	22.5	31.5	88.9
Chen et al.[27]	Iron	-	5.6	13.7	24.2	35.4	-
Behera et al.[32]	Lead–zinc	-	11.75	22.48	37.92	50.73	89.13
Zhang et al.[62]	Gold	3.42	4.2	11.3	22.5	31.0	96.8
	Gold	2.8	4.1	10.8	20.4	27.6	93.6
Landriault[92]	Polymetallic	3.7	3.7	10.8	22.4	32.5	121.5
	Silica	2.7	1.9	9.0	22.5	31.5	88.9

of 75 m (height), 25 m (length), and 20 m (span) having side exposure. The OPC is currently used at 10–13% weight proportion which now has become an economic constraint to the mine management. Therefore, the laboratory investigations were undertaken to evaluate the strength of paste backfill mixture prepared by partial replacement of OPC with fly ash. At first, the experiments were performed to test the unconfined compressive strength (UCS) of the paste fill specimens of different mix configurations. Subsequently, the BN was employed to get the sensitivity of the variables and the degree of uncertainty in the strength development to find out the most appropriate mix proportion. This section explains the study samples (Section 2.1), experimental program (Section 2.2), method of Bayesian network construction (Section 2.3), and validation technique (Section 2.4).

2.1 Samples of the Study

The samples of mill tailings (MT), OPC, and fly ash (FA) were collected and their physical and chemical characteristics were determined prior to preparing CPB and presented in Section 3. An extensive review has been carried out on the physical and chemical characteristics of the previous reported mill tailings, OPC, and fly ash and their subsequent effect on the CPB's performance. The outcome of the review is presented in the subsections below.

2.1.1 Mill Tailings

The physical and chemical characteristics of the mill tailings can have a great influence on the CPB's strength gain [38, 85]. These characteristics significantly vary with the host rock properties, extraction, and ore recovery methodology [86]. There is no distinctive categorization system of mill tailings due to its broad characteristics. Hence, each type of tailings demands the unique design of the CPB system which could not be generalised [87–91]. Depending on the weight% of particles finer than 20 µm, mill tailings are termed as coarse (15–35%), medium (35–60%), and fine tailings (60–90%) [92]. The well-graded tailings have a positive impact on the mechanical characteristics of the CPB [9, 16, 21, 86, 87]. Particles of the mill tailings are in general angular shaped and have a rough texture probably due to blasting and processing of the ore rock [32, 87]. The specific gravity and the mean particle diameter (D_{50}) of the mill tailings vary between 2.7–3.4 and 20–30 µm, respectively, as reported in various studies (Table 3).

The mill tailings have been found to contain varying proportions of the oxides of Si, Ca, Al, Fe, Mg, S, Na, Pb, and Zn, depending on their origin. Table 4 shows that few researchers have reported the abundance of silicate which increases the abrasiveness of the particles and may lead to high-friction losses during pipeline transportation of CPB. However, the presence of silica densifies the pore structure of CPB by reducing its porosity [93–95] and improves its water retention potential [8, 29] and strength properties [32, 55]. The oxides of Ca, Al, Fe, and Mg result in good binding ability [27] but the sulphur deteriorates the strength due to oxidisation and concomitant formation of sulphate products [61, 87]. The high sulphur content may result in free expansion ratio at a later age and result in specimens collapse due to cracks [87]. Based on the reactivity of the sulphide minerals, they can be placed in the following order: pyrrhotite > arsenopyrite > pyrite > chalcopyrite > sphalerite > galena > chalcocite [96]. Benzaazoua et al. [58] found that the OPC is the only suitable binder in the paste fill prepared with high sulphide mill tailings. The strength of the paste fills can increase up to a critical limit of the sulphur content and further increase in sulphur results in the loss of strength [26]. The strength growth can be better in the CPB prepared with artificial silica tailings as it can well control the geotechnical, chemical, and mineralogical characteristics [7].

2.1.2 Binder

The backfill strength development is directly dependent on the binder category, dosage and its potential to resist

Table 4 Chemical composition of previously reported mill tailings

Reference	Si	Al	Ca	Fe	Mg	Na	Pb	S	K	Zn
Yilmaz[9]	-	2.8	0.57	27.4	-	0.3	0.1	20.6	0.2	0.35
Célestin and Fall[21]	99.8	0.1	0.01	0.01	-	0.01	-	-	-	-
Fall and Pokharel[26]	99.8	0.05	0.01	0.035	0.01	0.01	-	-	0.02	-
Chen et al.[27]	63.58	5.55	11.4	6.19	9.11	-	-	-	-	-
Yilmaz et al.[29]	3.26	1.44	0.74	43.67	0.45	-	-	-	0.14	-
	10.88	3.9	1.43	57	1	-	-	-	0.24	-
Behera et al.[32]	33.34	12.13	17.42	16.58	6.43	0.49	-	10.43	1.73	-
Benzaazoua et al.[58]	10.12	2.63	1.07	26.8	0.21	-	-	32.2	-	0.045
	15.7	4.87	0.99	20.6	0.35	-	-	24.4	-	0.0002
	15.3	4.065	1.44	20.7	2.695	-	-	15.9	-	0.1795
	26.29	5.64	1.17	5.13	0.57	-	-	5.2	-	0.0149
Hane et al.[61]	15.1	1.5	0.1	21.2	0.1	0.4	-	20.2	0.6	-
Fall et al.[86]	99.8	0.1	0.01	0.01	-	0.01	-	0.0	-	-
	-	6.8	1.1	6.3	-	0.7	-	5.4	-	-
	13.4	3.1	0.8	31.1	-	0.8	0.2	30.1	-	-
Ercikdi et al.[87]	13.96	3.85	2.05	46.83	2.31	0.22	-	-	0.14	-
	11.12	2.2	1.58	49.47	1.9	0.18	-	-	0.08	-
Yin et al.[97]	21.58	8.69	0.51	24.99	3.05	-	-	3.64	0.875	-
Qui et al.[98]	20.91	3.22	44.41	16.39	11.3	-	-	2.23	0.52	-
Dong et al.[99]	27.51	3.64	29.86	8.70	19.7	0.88	0.16	4.96	1.08	0.44

detrimental chemical reactions [58]. The OPC remains the main binder constituent, but due to its significant cost [34] researchers have made several attempts with alternate binders like fly ash, silica fume, slag, jarosite, and pumice to attain the desired strength of the CPB [19, 30, 32, 39, 100–102]. Based on the particle shape, fineness, and chemical composition, the binders can affect the paste fills' strength development. The addition of fly ash to the CPB reduces the binder cost, improves the packing density, and avoids pipeline blockage by reducing the total average particle size [62, 103]. The rate of strength gain someway decreases with increasing the replacement level of OPC with alternate binders [19, 32, 64, 102, 104, 105]. It is because the chemical reactivity of these binders is significantly less in comparison to the OPC as explained by Singh et al. [19] by determining hydration index, and Behera et al. [102] by calculating the ratio of lime to that of percentage of silica, alumina, and iron oxide. The chemical compositions of the OPC and fly ash as reported by previous authors are summarised in Table 5. The OPC contains the highest proportion of the oxide of the Ca followed by the oxide of the Si and Al. The presence of Ca helps in quick hydration and formation of cement gel products and hence shows the good binding ability of the material. The Ca oxide in the fly ash is observed to be very low and Si oxide is found to be quite high which resulted in less degree of pozzolanic activity and high degree of water retention potential in comparison with the OPC.

2.2 Test Parameters and Procedures

The CPB mixes were prepared by varying the proportion of mill tailings, OPC, and fly ash. The paste fill specimens are termed here as 'control' specimens when prepared without fly ash addition and 'fly ash mixed' specimens when OPC is replaced partially with the fly ash. The control group of CPB were designed to acquire the targeted strength 1 MPa at the age of 28 days. The OPC was subsequently replaced with the fly ash with a maximum limit up to 4% by weight.

The CPB ingredients were mixed thoroughly at a fixed water percentage and then cylindrical moulds of dimension 100 mm (diameter)*200 mm (length) were casted to estimate the compressive strength. The specimens were demoulded at the age of 24 ± 1 h and thereafter cured in a humidity chamber at a constant temperature (30 ± 1 °C) and relative humidity of 80 ± 3 °C up to the predefined age of test. The compressive strength was measured at 7, 14, 28, and 56 days. The two ends of the samples were first planned to get their surfaces normal to the plates of the mechanical press prior to the tests. The specimens were subjected to a constant deformation rate of 1 mm/min (ASTM C 39) [106] for determining the UCS. The failure patterns of the specimens are shown in Fig. 2. Most of the specimens were observed to follow hourglass type of failure and in a few cases column-shaped failure, cone-shaped failure, and distributed-type failure with a number of vertical and shear cracks were also observed. For each mix design, 3 samples

Table 5 Chemical composition of previously reported OPC and fly ash

Binder	Reference	Si	Al	Ca	Fe	Mg	S	K	Na	Ti
OPC	Yilmaz [9]	19.51	4.86	65.76	-	2.21	3.67	-	-	-
	Célestin and Fall [21]	18.03	4.53	62.82	2.7	2.65	3.82	-	-	-
	Yilmaz et al. [29]	32.37	8.91	44.02	3.83	1.41	1.99	-	-	-
	Hane et al. [61]	16.6	5.14	67.80	3.4	2.19	6.24	1.06	-	-
	Wu et al.[71]	18.03	4.53	62.82	2.7	2.65	3.82	-	-	-
	Yin et al. [97]	19.32	6.14	59.24	3.15	1.24	-	1.12	-	-
	Moghaddam et al. [104]	19.23	5.12	64.26	2.86	1.28	2.73	0.51	0.18	0.31
	Sevim and Devir [105]	21	5.38	62.1	3.22	1.98	3.11	0.81	0.39	-
	Qui et al. [98]	22.86	5.45	60.51	3.35	1.57	3.01	0.56	-	-
	Dong et al. [99]	42.53	0.06	40.36	6.23	4.18	-	1.25	-	-
	Behera et al. [32]	60.71	27.27	2.08	4.61	0.56	0.86	1.05	0.39	1.67
	Zhang et al. [62]	51.92	19.03	1.0	3.87	1.18	-	1.47	0.54	-
Fly ash	Qi et al. [98]	52.42	32.48	3.05	3.62	1.01	-	-	-	1.26
	Moghaddam et al. [104]	59.21	28.11	2.48	3.68	0.53	-	1.18	0.63	1.11
	Sevim and Devir [105]	60.06	26.97	3.00	3.65	0.59	-	1.24	0.62	1.05
		46.6	12.4	14.5	9.74	7.23	5.52	2.28	1.01	-

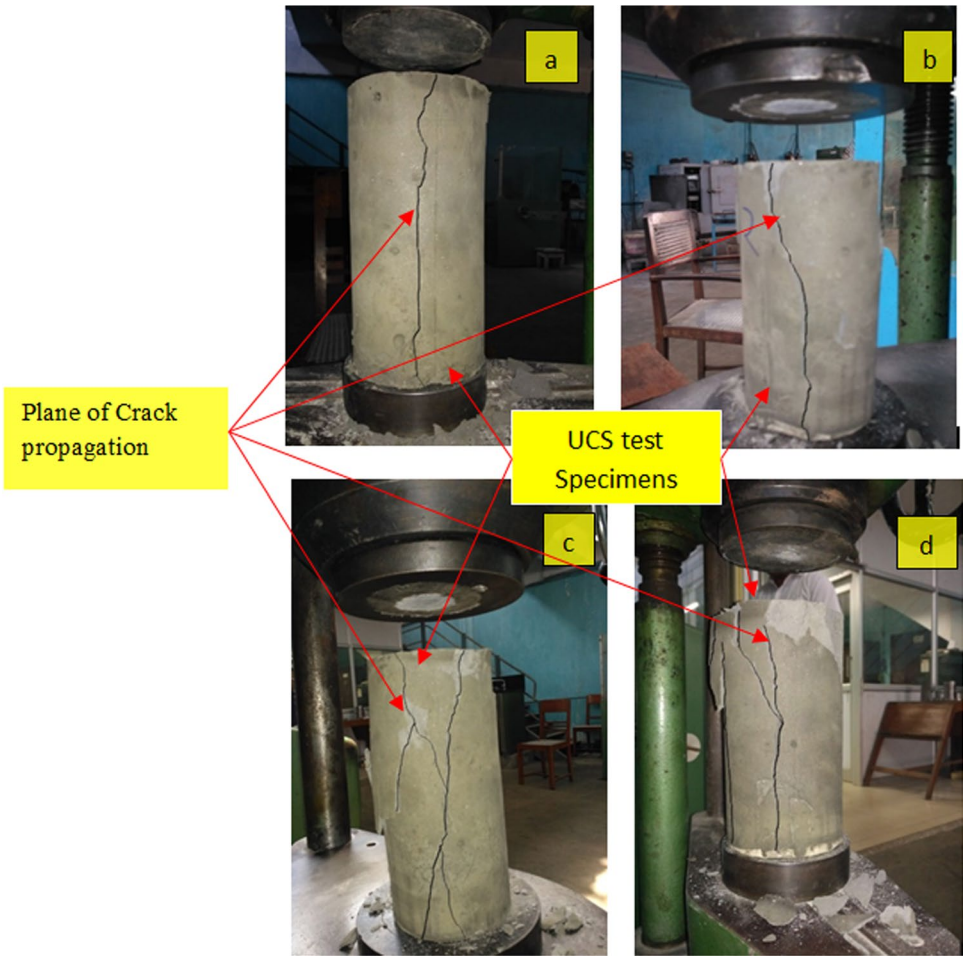

Fig. 2 Failure pattern of the CPB under uniaxial loading: **a** column-like mode of failure, **b** cone-type failure with an initial localisation failure in the central part of the specimen, **c** hourglass-type failure, **d** distributed-type failure with prominent vertical splitting cracks with a number of shear cracks

were tested at the specified curing age and their average UCS values were taken and therefore 96 readings were tabulated.

Instantly after preparation of the fresh paste mix, the workability and bleeding tests were carried out. The slump test was performed for the workability in accordance with the ASTM C 143 [107] in a standard slump cone apparatus of 300-mm height with metal cone thickness 1.6 mm having top and bottom diameters of 100 mm and 200 mm, respectively. The slump test measures the consistency of the fresh paste before it sets. The bleeding of the paste mix was measured as per the procedure laid down in the ASTM C 232–09 [108].

2.3 Bayesian Network Model: Building Model Structure

The causal interrelationship among the variables can be proficiently modeled with the Bayesian networks (BNs) [109, 110]. It is a directed acyclic graph that consists of two parts: a quantitative and a qualitative part. The nodes and arrows descend underneath the qualitative part [111], whereas the conditional probability tables (CPTs), which are used to determine the probability distribution of each state of variables in respect of their parent states, constitute the quantitative portion. For a given set of nodes, $X = [X_1, X_2, X_3, \ldots X_n]$, the CPT can be quantified as:

$$P(X_1, X_2, \ldots, X_n) = \sum_{i=1}^{n} P\left(\frac{X_i}{Parent(X_i)}\right) \quad (1)$$

The construction of BNs starts with defining the network structure which is a directed acyclic graph, and represents causal dependency among the variables. The model can be constructed in two ways: first by using the structure learning algorithm [112, 113] and in the second approach, the experts are asked to assign a causal relationship for each pair of variables [111, 114, 115]. Rivas et al. [116] concluded that there are not any significant differences between the models built with expert's knowledge and structure learning algorithm. Since the construction of the model with expert's opinion is somehow a complex and extensive process (see Fam et al. [111] for more details), therefore, the present study considered the structure learning algorithm feature to learn the model structure. Although there are a variety of algorithms available to graphically represent the conditional independence assumption but, with due attention imparted to the findings of Li et al. [77] and Feng et al. [79] (who reported TAN classifier and naïve Bayes classifier as the best performing tools in their respective investigation), in the current study naïve Bayes and TAN classifiers were selected for classification with BN model. The significance of these two classifiers towards paste fill strength was initially compared and then the model with highest reliable classifier was identified for subsequent analysis.

Once the model structure is defined, it is trained by employing the dataset and then the conditional probability table (CPT) of the model is formed. The expectation maximization (EM) algorithm is often preferred by the researchers to estimate the CPT [117, 118]. The EM algorithm alternates between expectation and maximization step and the dataset is completed by maximum likelihood estimation (MLE) of the model parameter (θ). In the maximization step, the dataset is employed for the new MLE, θ', and the iteration continues up to a prefixed number of iterations.

Table 6 Confusion matrix for binary classification

		Predicted	
		Negative	Positive
Actual	Negative	TN	FP
	Positive	FN	TP

2.4 Model Performance and Validation

The next step after model learning is to determine and validate its classification ability. This could be done by estimating error rate and kappa value once the confusion matrix is formed [119]. There are also several model performance indicators such as logarithmic loss, quadratic loss, receiver operating characteristics curves, and spherical pay-off which are widely practised to validate the BN model [79, 104, 111, 118–121]. Thus, based on the earlier practices and recommendations, these indices are selected to evaluate the performance of the present developed model. The detailed explanation of these indices is given in the following sub-sections.

2.4.1 Confusion Matrix

It is a table which outlines the performance of a classifier structure algorithm. For the binary classification, the confusion matrix can be expressed as follows (Table 6):

The confusion matrix defines the performance of the model in terms of the predicted and actual values. The term "TN" stands for true negative which signifies the number of negative values captured accurately. The term "TP" is an abbreviation of true positive which states the number of positive values classified accurately. The term "FP" means false positive which is the count of actual negative cases classified as positive, whereas "FN" is an indication of false negative, i.e. the number of actual positive values classified as negative.

2.4.2 Accuracy and Error Rate

Accuracy is the most commonly used index in classification process. The below equation is used to calculate the accuracy with the help of confusion matrix.

$$Accuracy = \frac{TN + TP}{TN + FP + FN + TP} \tag{2}$$

Alternatively, the accuracy can also be expressed as:

$$A_c = \left[\frac{\sum_{i=1}^{n} m_{ii}}{\sum_{i,j=1}^{n} m_{ij}}\right] \times 100\% \tag{3}$$

m_{ij} is the element of the i^{th} row and j^{th} column in the confusion matrix.

The error rate can be calculated as follows: Error rate = 1- accuracy.

2.4.3 Kappa Value

Kappa statistics is first introduced in 1960 by Jacob Cohen to measure the interobserver agreement [122]. Landis and Koch [123] have provided the interpretation of the kappa values in the following order: less than 0 (no agreement), 0 to 0.20 (slight), 0.21 to 0.40 (fair), 0.41 to 0.60 (moderate), 0.61 to 0.80 (substantial), and 0.81 to 1.0 (perfect). The kappa index is broadly practised statistical tool to validate the performance of the model [124]. The following example may be helpful in understanding the determination of the kappa value:

Assume that two observers independently allocate x number of objects among n mutually exclusive classes. To estimate the agreement among the two observers, initially a square contingency table ($A = [a_{lm}]$) where a_{lm} indicates the number of objects placed in category l by the first observer and in category m by the second observer (l, $m \in [1, 2,..., x]$). If the categories of the observers are in the same order, then the diagonal elements (a_{ll}) of A reflect the number of objects placed in the same categories by both observers (the agreement). Let $C = (c_{lm})$ be the corresponding table of proportions with relative frequencies $c_{lm} = a_{lm}/x$. Therefore, the row and column totals can be given by:

$$c_l = \sum_{m=1}^{x} c_{lm} \text{ and } d_l = \sum_{m=1}^{x} c_{ml}$$

c_l and d_l are the marginal totals of C. The kappa coefficient (k) is defined as

$$k = \frac{C - E}{1 - E} \tag{4}$$

where, $C = \sum_{l=1}^{x} c_{ll}$ and $E = \sum_{l=1}^{x} c_l d_l$

2.4.4 Scoring Rules

In addition to determining confusion matrix, another way to test and validate the performance of the model is the scoring rules [119]. The logarithmic loss, quadratic loss, and spherical pay-off are few common parameters of the scoring rules [125]. The range of logarithmic loss is from 0 to infinity and a lower value signifies better performance of the model [104, 119–121, 126]. The value of quadratic loss ranges between 0 and 2 and a lower value indicates consistency in the performance [111]. The spherical pay-off varies among 0 to 1, and a higher value implies the well-performing ability of the model [111]. The mathematical expression of the logarithmic loss, quadratic loss, and spherical pay-off can be given as follows:

$$Logarithmic\ loss = M(-\log\left(P_c\right) \tag{5}$$

where M is the mean over all test cases and P_c is the probability of the correct state.

$$Quadratic\ loss = M\left(1 - 2 \times P_c + \sum_{j=1}^{n} P_j^2\right) \tag{6}$$

where P_j is the probability of the predicted state and n is the number of states.

$$SP = MOAC.\frac{P_c}{\sqrt{\sum_{j=1}^{n} P_j^2}} \tag{7}$$

where, SP = spherical pay-off index, MOAC = mean probability value of a given state averaged over all cases; P_c = predicted probability of the correct state; P_j = predicted probability of the state j; n = total number of states.

2.4.5 Receiver Operating Characteristics (ROC) Curve

The ROC curve is one of the indexes which depict the performance of the BN model [127, 128]. A ROC curve plots per cent true positives as a function of per cent false positives [129]. The area under the ROC curve varies from 0 to 1, where values between 0.5 and 0.7 designate poor discriminating ability, between 0.7 and 0.9 indicate practical classification ability, and value 1 be a sign of perfect performance, i.e. 0% false positive cases [121, 130–132].

2.4.6 Sensitivity Analysis

The performance of the BN could also be calculated by means of sensitivity analysis. This is the unique feature of the BN to update the belief by estimating sensitivity of one target node towards different causal factors. Therefore, the

Table 7 Particle size analysis results of OPC and fly ash

Parameters	G_S	Colour	D_{90}	D_{60}	D_{50}	D_{30}	D_{10}	C_u	SSA (m^2/kg)
Mill tailings	2.89	Dark grey	177.059	66.993	49.996	24.805	6.868	9.75	346.6
OPC	3.1	Light grey	61.626	30.756	25.661	17.464	9.583	3.21	412.9
Fly ash	1.84	Medium grey	144.155	50.027	37.465	19.853	7.963	6.28	460.7

*SSA: Specific Surface Area

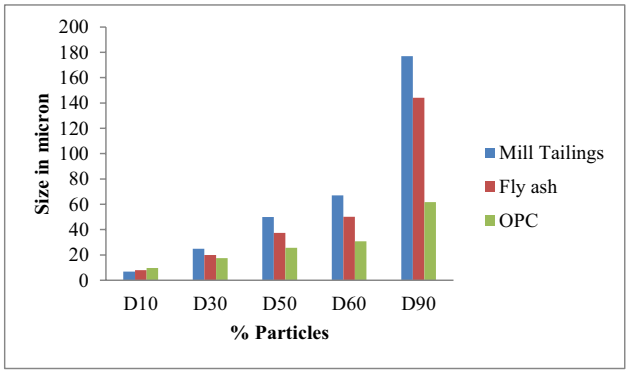

Fig. 3 Particle size distribution results of samples

predictors could be prioritised based on their relative significance. The sensitivity analysis is measured with mutual information (MI) and variance reduction [133]. The MI which assess the extent of information shared between two variables with a higher value is an indication of stronger dependence [126, 134, 135]. The equation to calculate the MI between two variables is shown as follows:

$$MI = \sum_{x,y} p(x,y) log \frac{p(x,y)}{p(x).p(y)} \quad (8)$$

where, $p(x,y)$ is the joint probability density function of variables X and Y, and $p(x)$ and $p(y)$ are the marginal probability density functions of X and Y, respectively.

3 Result and Discussion

3.1 Sample Characteristics

The results of particle size distribution of study samples are shown in Table 7 and Fig. 3. The mill tailings used in the present study were lead–zinc tailings of dark grey colour. The specific gravities of the mill tailings, OPC, and fly ash were obtained as 2.89, 3.1, and 1.84 in that order. The mean particle diameter of the OPC (25.661 µm) was found to be less than that of fly ash (37.465 µm) and mill tailings (49.996 µm). Table 10 shows that the 10% particles of the mill tailings, OPC, and fly ash are finer than 6.868 µm, 9.583 µm, and 7.963 µm, whereas 90% of the particles are finer than 177.059, 61.626, and 144.155 µm. The results were further used to determine the coefficient of uniformity (Cu) which determines the size gradation of particles and expressed as the ratio of D_{60}/D_{10}. The well-graded soil exhibits Cu greater than 4 to 6 and uniformly graded soils have a Cu less than 4. The values of Cu for the mill tailing, OPC, and fly ash were 9.75, 3.21, and 6.28. Accordingly, the mill tailings can be characterised as well as graded than OPC and fly ash and having the finest size of particles. The OPC was found to contain fine particles of a comparatively uniform size range than that of fly ash.

The chemical compositions of the mill tailings, OPC, and fly ash are presented in Table 8. It shows that the mill tailings are silicate type in nature as the oxides of Si (47.46%) are the most abundant followed by the oxides of Al (17.1%), S (13.46%), and Fe (11.31%), and minor proportions of Mg (3.53%), K (3.14%), Ca (1.8%), Na (1.37%), Ti (0.59%), and P (0.26%). The OPC contains the highest proportion of the CaO (61%), followed by SiO_2 (17%), Al_2O_3 (8%), Fe_2O_3 (6%), MgO (4%), SO_3 (3%), K_2O (0.7%), and Na_2O (0.3%). The similar pattern of the chemical composition ($CaO > SiO_2 > Al_2O_3 > Fe_2O_3 > MgO > SO_3 > K_2O > Na_2O$) was also reported in the previous studies as summarized in Table 4 except to that reported by Hane et al. [61] and Dong et al. [99]. Table 8 demonstrates that the fly ash contains abundance of SiO_2 (57.04%) followed by Al_2O_3 (26.89%), Fe_2O_3 (12.47%), CaO (1.4%), K_2O (0.83%), MgO (0.52%), SO_3 (0.36%), P_2O_5 (0.19%), and TiO_2 (0.08%). The oxides of Si, Al, and Fe together contribute around 96% of the total chemical composition of the fly ash. Behera et al. [32], Zhang et al. [62], Qi et al. [98], and Moghaddam et al. [104] also stated the oxides of Si, Al, and Fe as three major ingredients of fly ash with collective proportions of 92.59%, 74.82%, 88.52%, and 91% in their respective studies. Based on the chemical composition of the studied samples, hydration index (HI) was calculated. It is a significant parameter that describes the chemical reactivity of the pozzolans. The reactivity will be termed as good for HI value greater than 1 [136]. Mathematically, the HI can be expressed by the following equation:

Table 8 Chemical composition of mill tailings, OPC, and fly ash samples

Chemical composition	SiO_2	Al_2O_3	Fe_2O_3	TiO_2	CaO	MgO	P_2O_5	SO_3	Na_2O	K_2O	(HI)
Mill tailings	47.46	17.1	11.31	0.59	1.8	3.53	0.26	13.46	1.37	3.14	0.19
OPC	17	8	6	-	61	4.0		3	0.3	0.7	3.03
Fly ash	57.04	26.89	12.47	0.08	1.4	0.52	0.19	0.36	0.21	0.83	0.15

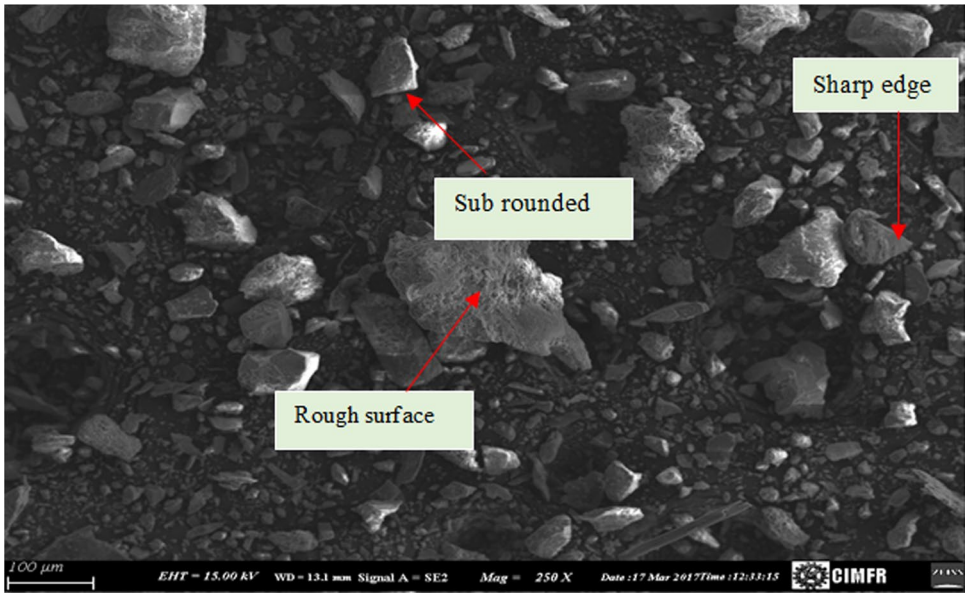

Fig. 4 Microscopic image of mill tailings

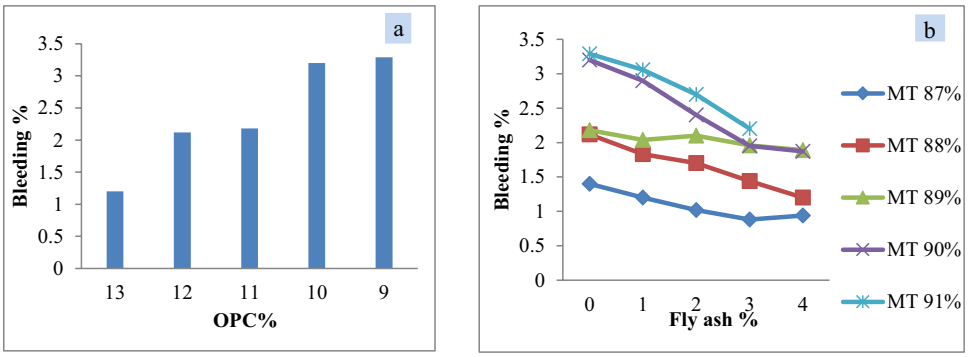

Fig. 5 Bleeding rate of CPB specimens **a** for control mix and **b** for fly ash–added mix

$$HI = \frac{CaO + MgO + \frac{1}{3}Al_2O_3}{\frac{2}{3}Al_2O_3 + SiO_2} \quad (9)$$

It can be seen from Table 8 that the HI values for the mill tailings, OPC, and fly ash are 0.19, 3.03, and 0.15. Accordingly, it can be termed here that the chemical reactivity of the OPC is about 20 times more than that of fly ash. Furthermore, it can be seen from the Fig. 4 that the particles of mill tailings are rough in texture and sub-rounded with sharp edges as found through the scanning electron microscopic (SEM) study.

3.2 Properties of Fresh CPB

3.2.1 Bleeding Test

The paste aggregates start to settle at the bottom of the moulds just after placing and water (at a very low rate) is accumulated at the surface of the fresh CPB, called bleeding. Bleeding capacity of paste mixtures was determined as per the procedure laid down in the ASTM C232-09 [92]. The test results of water loss through bleeding are presented in Fig. 5a and b. It indicates that the bleeding percentage

increased with decreasing OPC content in the CPB for control specimens. The increased bleeding can be attributed to the high water retention potential of the OPC; hence, it absorbs more water during the hydration process and thus less quantity of free water is available in the inter particle voids to drain out in the form of bleeding. Figure 5b illustrates that at a fixed mill tailings proportion, the replacement of OPC with that of fly ash lessens the volume of bleed water. It could also be seen from Fig. 5 that increasing solid percentage of the mill tailings from 87 to 91wt% increases the volume of bleed water. The reason could be that the CPB is prepared at a constant solid proportion (72wt%). Therefore, the increasing solid content of mill tailings lessens the space for the binders (OPC + fly ash). Since the mill tailings retain less water in comparison to the binders, therefore the quantity of free water in the CPB matrix will increase which in turn increases the bleeding rate.

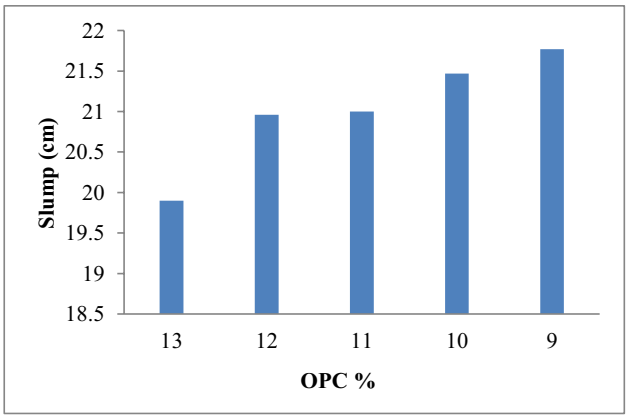

Fig. 6 Slump with OPC % at no fly ash

3.2.2 Workability

The test results of slump and spread with ± 1-mm error range for each mix configuration are presented in Table 9 for the control group and fly ash replacement group. The slump and spread were found to increase with lessening cement content as could be seen from Fig. 6. The slump and spread of the CPB were further observed to upsurge gradually with escalating replacement level of the OPC with that of fly ash. It may be attributed to the enhanced lubrication effect with the addition of fly ash. The particle size distribution of the mix ingredients, binder type and quantity, and solid:water ratio strongly influence

Table 9 Variation of slump and spread with for CPB mix

Water %	Solid %	MT %	OPC %	Fly ash	Pulp density (t/m^3)	Slump (mm)	Spread (mm)
28	72	87	13	0	1.95	199	355
28	72	88	12	0	1.93	203	359
28	72	89	11	0	1.92	204	365
28	72	90	10	0	1.89	208	363
28	72	91	9	0	1.87	213	368
28	72	87	12	1	1.93	201	339
28	72	87	11	2	1.94	200	340
28	72	87	10	3	1.90	203	346
28	72	87	9	4	1.88	205	345
28	72	88	11	1	1.90	202	339
28	72	88	10	2	1.89	204	340
28	72	88	9	3	1.86	207	341
28	72	88	8	4	1.85	208	345
28	72	89	10	1	1.89	205	335
28	72	89	9	2	1.87	208	337
28	72	89	8	3	1.85	208	345
28	72	89	7	4	1.82	209	-
28	72	90	9	1	1.86	210	346
28	72	90	8	2	1.84	209	348
28	72	90	7	3	1.83	211	349
28	72	90	6	4	1.82	212	334
28	72	91	8	1	1.84	211	346
28	72	91	7	2	1.83	214	348
28	72	91	6	3	1.81	214	349

Table 10 Strength (UCS) value for different paste fill composites

Mill tailing, 87%				Mill tailing, 88%				Mill tailing, 89%				Mill tailing, 90%				Mill tailing, 91%			
OPC	FA	Days	UCS	OPC	FA	Days	UCS	OPC	FA	Days	UCS	OPC	FA	Days	UCS	OPC	FA	Days	UCS
13	0	7	1.93	12	0	7	1.74	11	0	7	1.41	10	0	7	1.1	9	0	7	0.81
13	0	14	2.25	12	0	14	2.15	11	0	14	1.67	10	0	14	1.36	9	0	14	0.86
13	0	28	2.75	12	0	28	2.53	11	0	28	1.83	10	0	28	1.64	9	0	28	1.03
13	0	56	2.97	12	0	56	2.72	11	0	56	2.01	10	0	56	1.89	9	0	56	1.09
12	1	7	1.77	11	1	7	1.53	10	1	7	1.15	9	1	7	0.87	8	1	7	0.63
12	1	14	2.05	11	1	14	1.66	10	1	14	1.22	9	1	14	0.95	8	1	14	0.71
12	1	28	2.61	11	1	28	1.89	10	1	28	1.46	9	1	28	1.14	8	1	28	0.78
12	1	56	2.78	11	1	56	2.06	10	1	56	1.57	9	1	56	1.25	8	1	56	0.92
11	2	7	1.58	10	2	7	1.24	9	2	7	0.91	8	2	7	0.69	7	2	7	0.51
11	2	14	1.74	10	2	14	1.31	9	2	14	0.98	8	2	14	0.77	7	2	14	0.59
11	2	28	1.97	10	2	28	1.54	9	2	28	1.21	8	2	28	0.83	7	2	28	0.63
11	2	56	2.12	10	2	56	1.59	9	2	56	1.26	8	2	56	0.94	7	2	56	0.81
10	3	7	1.22	9	3	7	0.98	8	3	7	0.78	7	3	7	0.54	6	3	7	0.41
10	3	14	1.37	9	3	14	1.04	8	3	14	0.86	7	3	14	0.68	6	3	14	0.46
10	3	28	1.59	9	3	28	1.27	8	3	28	0.91	7	3	28	0.77	6	3	28	0.68
10	3	56	1.71	9	3	56	1.32	8	3	56	0.99	7	3	56	0.82	6	3	56	0.77
9	4	7	1.08	8	4	7	0.84	7	4	7	0.62	6	4	7	0.48	-	-	-	-
9	4	14	1.17	8	4	14	0.89	7	4	14	0.74	6	4	14	0.57	-	-	-	-
9	4	28	1.36	8	4	28	1.06	7	4	28	0.8	6	4	28	0.73	-	-	-	-
9	4	56	1.49	8	4	56	1.12	7	4	56	0.86	6	4	56	0.79	-	-	-	-

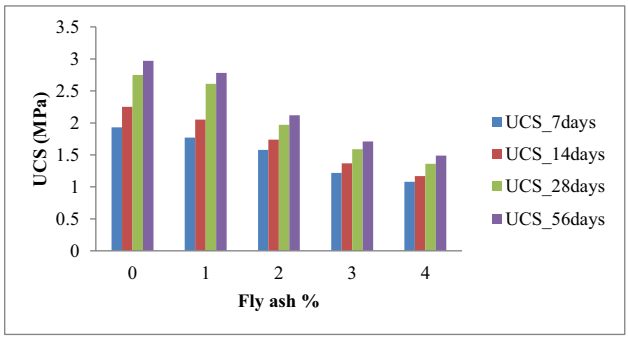

Fig. 7 Strength variations with binders (OPC and FA) for 87% mill tailings group

the consistency of the CPB or concrete [104, 137–139]. Behera et al. [32] designed their CPB mix with a 195-mm slump at a solid:water ratio of 77:23 for 8 wt% binder category. They found increase in slump value when binder dosage was reduced to 5 wt%. Therefore, to maintain the required consistency (195-mm slump) of the CPB for 5 wt% binder group, they further enhanced the solid proportion from 77 to 78 wt%. Moghaddam et al. [104] observed that the flow characteristics of the blended cement paste improve with increasing the proportion of fly ash. The spherical shape, glassy and smooth surface, and higher lubrication effect are few significant factors which enhance the workability of the paste with addition of fly ash [104]. Similarly, the investigation carried out by Mora et al. [137], Ferraris et al. [138], and Patel et al. [139] for different paste/mortar/concrete shows the improvement in the workability with increased proportion and fineness level of binders. Ferraris et al. [138] tested six different mineral admixtures and found that the ultrafine fly ash (UFFA) gives the best result in improving the concrete flow. Patel et al. [139] also observed the improvement in workability of the self-compacting concrete with increased proportion of the binder. The density of fresh paste fill mix was further observed to decrease with increasing mill tailings and fly ash proportion and with lessening OPC content. By summarising these results, it can be concluded that the initial consistency and compactness of fresh CPB decrease with mill tailing and fly ash proportion.

3.3 Properties of Hardened CPB

The UCS test was carried out on the specimens of the entire 24 mix configurations at 7, 14, 28, and 56 days of curing and, in total, 96 readings were documented. The test results are presented in Table 10. The trends of the UCS with respect to the binder dosage and curing period are explained in the following subsections.

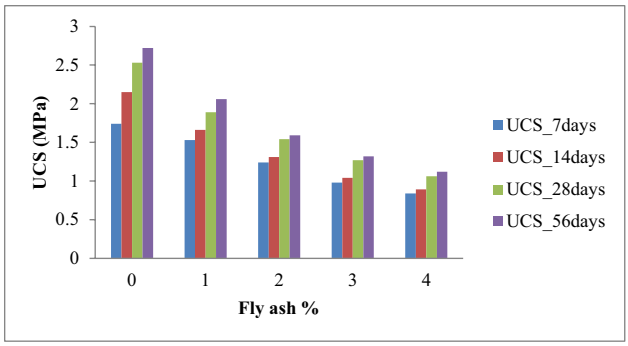

Fig. 8 Strength variations with binders (OPC and FA) for 88% mill tailings group

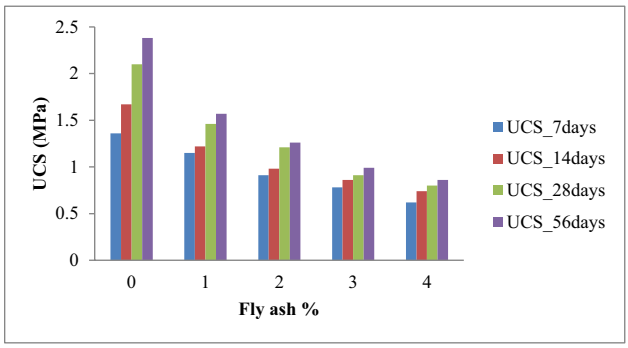

Fig. 9 Strength variations with binders (OPC and FA) for 89% mill tailings group

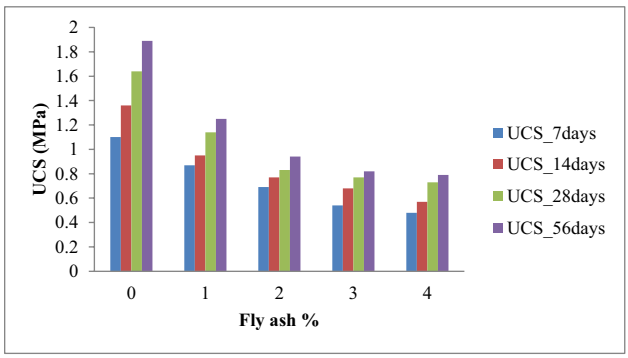

Fig. 10 Strength variations with binders (OPC and FA) for 90% mill tailings group

3.3.1 Effect of Binder Dosage on the UCS Development

The compressive strength test results of the paste specimens are shown in Figs. 7, 8, 9, 10, and 11. The strength was observed to decline almost linearly by adding fly ash in the CPB. It may be due to the low hydration index of the fly ash compared to the OPC. At 28 days of curing, all specimens of the control group surpassed the targeted strength 1 MPa.

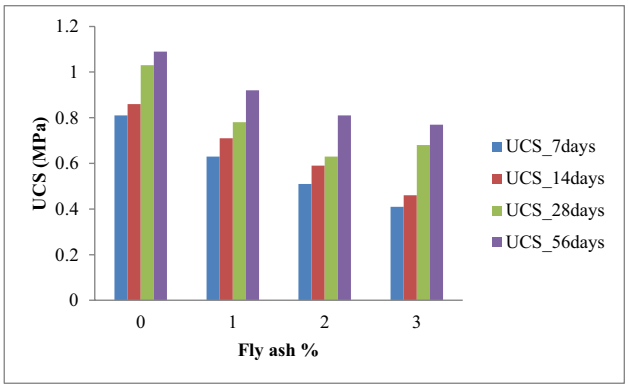

Fig. 11 Strength variations with binders (OPC and FA) for 91% mill tailings group

The 28-day strength developments within the control samples consisting 87%, 88%, 89%, 90%, and 91% mill tailings were 175%, 153%, 110%, 64%, and 3% higher than the targeted strength. The 28-day cured specimens prepared with 87% mill tailings and 1%, 2%, 3%, and 4% fly ash attended 161%, 97%, 59%, and 36% greater strength than the critical limit. For the specimens of 88% mill tailings group, the strengths were respectively 89%, 54%, 27%, and 6% higher in reference to the 1 MPa. Likewise at 89% mill tailings, the paste fill specimens up to 2% fly ash have crossed the 1-MPa mark, whereas 3–4% fly ash mixed specimens exhibited 9% and 20% low strength after completion of 28 days of curing phase. The optimal fly ash (FA) proportion was found to be 1% for the paste fill specimens of 90% mill tailings (MT). At 91% mill tailings, none of the fly ash mixed specimens could attain the targeted strength at 28 days of curing. Further at the curing ages of 7, 14, and 56 days, all the specimens mixed with fly ash displayed strength growth at a lower rate than their respective counterparts. The low strength development in the fly ash mixed specimens can be attributed to the fact that the pozzolanic activity of fly ash is lower than that of OPC; therefore, replacing the stronger binder with the weaker one deteriorates the strength by declining the formation of hydration products inside the matrix.

3.3.2 Effect of Curing Period on the UCS Development

Figure 12 depicts the percentage variation in strength growth with varying curing period from 7 to 14 days, 14 to 28 days, and 28 to 56 days. The curing period itself does not have any direct consequence on the strength development but is shows the rate of binder hydration and the formation of hydrated products inside the pores of the CPB structure. The strength development patterns for all the specimens were observed to be similar but the rate of strength gain was less in the fly ash mixed paste specimens than that of control paste specimens. For all the CPB

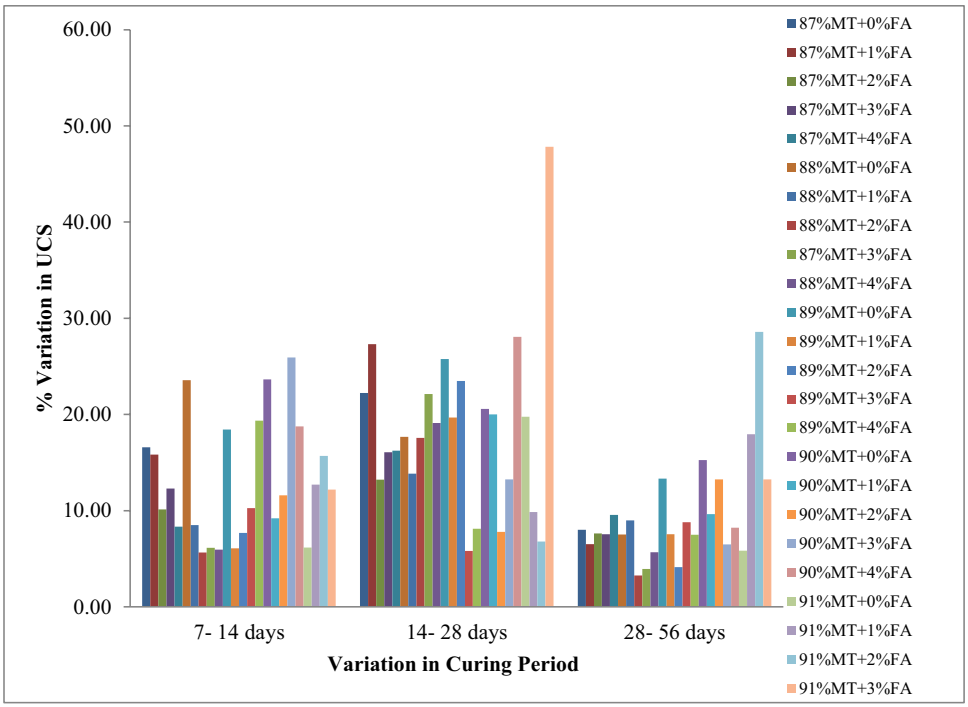

Fig. 12 Percentage variations in UCS against the curing period

specimens of the control group, the maximum percentage change in the strength was noticed during 7–14 days and 14–28 days. During 28–56 days of the curing phase, the change in the UCS was comparably low. It shows that the OPC results in quick hardening and the control specimens attained maximum fraction of their strength until 28 days of curing. In most of the cases, the paste specimens with added fly ash witnessed maximum strength variation during 14–28 days of curing phase. Therefore, the strengthening of CPB due to fly ash starts significantly after passing 14 days of curing. Only the paste specimens of 89% MT + 4% FA and 90% MT + 3% FA show the maximum rate of strength growth during 7–14 days of curing. The specimens of 90% MT + 2% FA, 91% MT + 1% FA, and 91% MT + 2% FA categories are observed to possess the maximum strength variation between 28 and 56 days. At 28 days of curing period, the control specimens of 87%, 88%, 89%, 90%, and 91% mill tailings have attained 92.6%, 93%, 88.2%, 86.8%, and 94% of their 56-day compressive strength. The fly ash mixed specimens also acquired more than 90% of their strength at 28 days except the specimens of 90% MT + 2% FA, 91% MT + 1% FA, and 91% MT + 2% FA configuration.

3.4 Bayesian Network Modelling: Coupled Interaction Approach

In the previous section, the conventional approach was presented to evaluate the strength with respect to the mix proportions. This section will illustrate the application and significance of the Bayesian network model to analyse the coupled effect of the variables on the strength. The subdivisions below will illustrate the categorisation of the datasets for feeding into the model, training and validation of the model, sensitivity of the variables, and finally the comparison between different joint strategies for recommending the most suitable mix proportions.

3.4.1 Categorisation of the Datasets

The experimental variables used here to train the BN model are continuous in nature. It is essential to discretize these variables first, before being used to train the BN [77, 79, 110, 126]. The discretization is aimed to determine the good cut points so that the datasets could be categorized into the intervals of an approximately equal number of observations. The discretization algorithm built-in software like WEKA is commonly used by the researchers for categorization of datasets [140], but we could not completely rely on the algorithm and final categorization is performed based on the practicality and assumptions which are to be investigated [77, 79]. Table 11 shows the final categorization of variables; the name of their states and the number of observations come under that category.

3.4.2 The "Trained" Bayesian Network Model

As explained in the Section 2.3, the Bayesian network is a directed acyclic graph between random *n*-dimensional

Table 11 Summary of the intervals employed for the parameters

Parameters		Set of intervals/frequency
Mill tailing proportion	Intervals	(87–88)/60, (89–91)/36
	States of mill tailing	MT87 to 88, MT89 to 91
Cement proportion	Intervals	(6–8)/36, (9–11)/48, (12–13)/12
	States of cement	Low, moderate, high
Fly ash proportion	Intervals	(0)/20, (1–2)/40, (3–4)/36
	States of ash	No, FA up to 2, FA 2to4
Curing days	Intervals	(7, 14)/48, (28)/, (56)/48
	States of curing days	Early age, middle age, later age
UCS	Intervals	(< 1.0)/41, (≥ 1.0)/55
	States of UCS	Less, high

variables. It can be defined as a pair (X, E) composed of random variables $X = (X_1, \ldots .., X_n)$ and directed acyclic graph (E). The graph composed of a set of n apexes (associated with the random variables$X_i, i = 1, 2, \ldots, n$) and a set of arrows between these apexes shows the association between these variables. The Bayes theorem defines the conditional independence relationship between the set of variables X_i and defines the prior probability. To model the conditional independence assumption between the study variables, the Bayes equation can be presented in the following manner:

$$P\left(\frac{Milltailings, cement, flyash, curingdays}{UCS}\right)$$

$$= \frac{P\left(\frac{UCS}{mill\ tailings,\ cement,\ fly\ ash,\ curing\ days}\right) P(mill\ tailings,\ cement,\ fly\ ash,\ curing\ days)}{P(UCS)} \tag{10}$$

where,

$P\left(\frac{Mill\ tailings,\ cement,\ flyash,\ curing\ days}{UCS}\right)$ = Prior probability of the predictors with respect to the given UCS value.

$P\left(\frac{UCS}{mill\ tailings,\ cement,\ fly\ ash,\ curing\ days}\right)$= Probability to acquire the certain value of UCS for the CPB specimen of given mix configurations and curing period.

$P(mill\ tailings,\ cement,\ fly\ ash,\ curing\ days)$ = Probability of the input variables. Also could be termed as overall mix recipe tried or overall experimental scenarios (Table 10).

$P(UCS)$ = Probability of the UCS of the CPB (Table 10).

Figure 13 shows the Bayesian network model, trained with the naive Bayes and TAN classifier structures. Both the models demonstrate the prior probability of the variables in terms of the existing experimental scenario (Table 10) of strength development inside paste fill specimens. The probability of strength gain is predicted as 57.1% (targeted value) and 42.9% (less than targeted value) by both the models. There is slight disparity between the models while predicting the prior probability of the mill tailings, cement, and fly ash and curing days with respect to the corresponding UCS value. Therefore, it is quite imperative to compare the predictive capability of both the models to identify the highest reliable classifier structure for the present study. This could be performed by forming confusion matrix and by estimating error rate and kappa value for both the classifiers. These indices have already been explained in Section 2.4; hence, their significance is interpreted here in terms of the CPB's strength development.

A confusion matrix is a table that describes the performance of a classifier on a cluster of test data. It shows the association or contradiction between the actual data and predicted data by the models. In terms of the strength gain of the paste fills, the terms of confusion matrix can be explained as follows:

True Negative (TN): The actual strength gain is less than 1 MPa and the model predicts it in an exact way.
True Positive (TP): The actual strength gain is equal to or greater than 1 MPa and the model predicts the alike.
False Positive (FP): The actual strength gain is less than 1 MPa but the model predicts it as high strength.
False Negative (FN): The actual strength gain is equal to or greater than 1 MPa but the model predicts it less.

Out of the total 96 experimental trials, in 55 cases, UCS was ≥ 1 MPa and in 41 cases it was less than 1 MPa (Table 10). For a total of 41 cases of UCS < 1 MPa, the naïve Bayes classified 36 cases as a true negative (UCS < 1 MPa) and 5 cases as a false positive (UCS ≥ 1 MPa), whereas the TAN classifier identifies all true negative cases in the exact same way. For the 55 positive cases of the strength (UCS ≥ 1 MPa), the BN developed with naïve Bayes and TAN structures classifies 4 cases and 33 cases as a FN (UCS < 1 MPa), respectively.

The terms FN and FP are considered the source of error in the model. The error due to FN cases up to a certain limit in the engineering design may be acceptable due to the rise in the safety factor [69]. In terms of the CPB's strength, the FN error shows that the model could not identify the

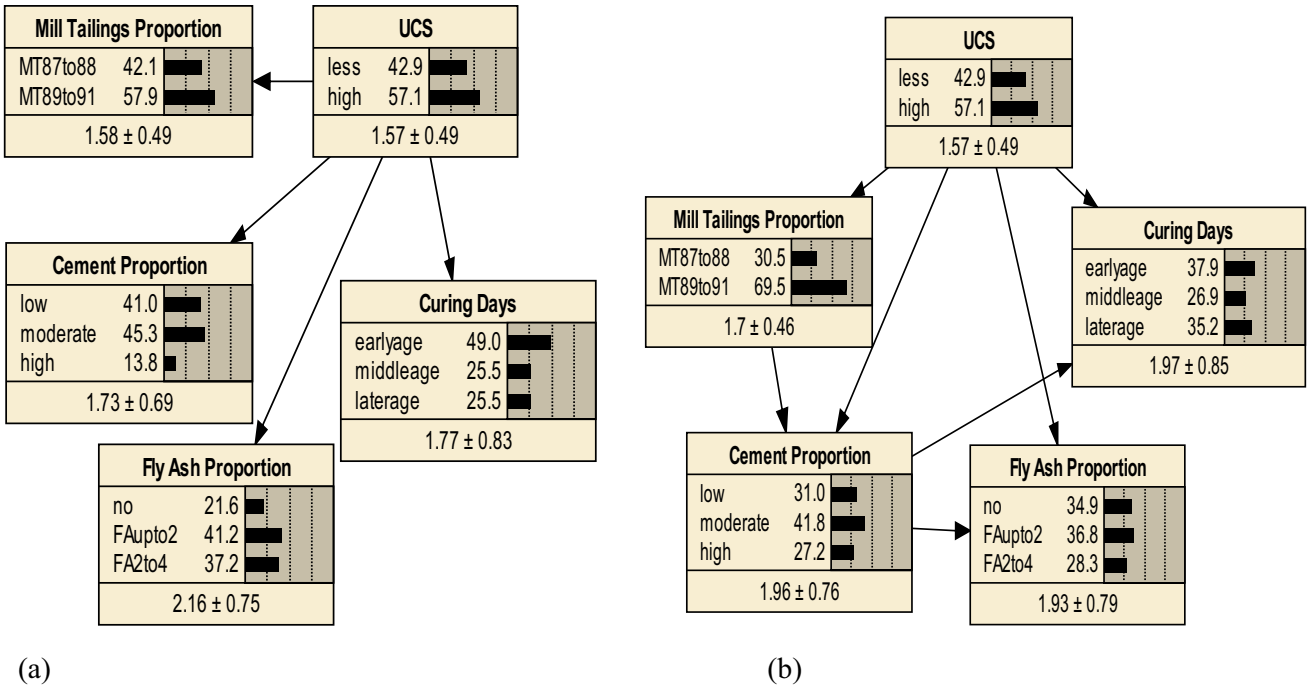

Fig. 13 Prior probability of variables with naive Bayes classifier (**a**) and TAN classifier (**b**)

positive cases of the UCS efficiently and to maintain the same strength, the binder (OPC) proportion is required to increase. For the fewer number of FN cases, the increment in OPC dosage may be marginal but high FN cases will unenviably necessitate to increase the binder dosage substantially and result in high operational cost. In contrast, the FP error overestimates the UCS by classifying CPB specimens of low strength (< 1 MPa) as high-strength specimens. Hence, the FP error ignores the threats in the experiments and possesses high risk of failure to the CPB structure.

It can be seen from the confusion matrix (Table 12) that the FN cases were the only source of error with the TAN classifier. The corresponding kappa values of the TAN classifier and naive Bayes classifier were 75 and 90.625. The kappa value shows the level of agreement between the experiment and the model. Hence, in context to the present study, this index is significant to determine the effectiveness of both the classifier structures to capture the trend in the experimental datasets. The comparison reveals that the naïve Bayes classifier can well capture the trend of the UCS development with respect to the mix configurations. Furthermore, the error rates with the naïve Bayes and TAN classifier were 9.375% and 25%, respectively. By summarising the above findings, it can be concluded that the naïve Bayes classifier can predict the CPB's strength in a more efficient way than that of the TAN classifier. Therefore, further analysis was carried out with the BN trained with the naive Bayes classifier structure.

Table 12 Confusion matrix of node "UCS" using two different classifiers

Classifier	Predicted			Error	Kappa
	Low	High	Actual		
Naive Bayes	36 (TN)	5 (FP)	Less	9.375	90.625
	4 (FN)	51 (TP)	High		
TAN	41 (TN)	0 (FP)	Less	25	75
	33 (FN)	22 (TP)	High		

The naive Bayes classifier shows that the prior probability to acquire the targeted strength was 42.9% for the paste fill specimens having mill tailings proportion between 87 and 88%. This probability is reduced to 33.3% when the mill tailings proportion varies between 89 and 91%. It shows that the increasing mill tailings proportion reduces the potential of paste fills to attain the requisite strength. The probability of failure to the CPB was 84.1% with 6–8% cement proportion which significantly reduced to the level of 13.6% and 2.3% for the moderate and high contents of cement. The prior probability of failure to the paste fill structure rises from 6.8 to 54.5% for varying the fly ash proportion from 'no fly ash' to '4% fly ash'. Similarly, the early age probabilities were 59.1% and 41.4% for the paste fill specimens to attain low and high strengths, respectively. The joint strategy feature to minimise the risk and to optimise the mix configuration has been explained in detail in Section 3.4.5.

3.4.3 Sensitivity Analysis

The sensitivity analysis was carried out to prioritise the influence of all predictors on the output node 'UCS'. The result is shown in Fig. 14. The variance reduction shows the degree of reduction in variance of the UCS when we look at other variables. The mutual information (MI) shows the amount of information shared between the two variables. In other words, MI determines how much our uncertainty about one causal factor is reduced when we have received some evidence about another causal factor. The higher MI between two variables signifies stronger association between them. The equation to calculate the mutual information is shown in Section 2.4.6. The interpretation of the MI in terms of the CPB's strength development could be comprehended by the following two assumed cases: (i) for the given UCS value of the CPB specimen, if we came to know mix composition (mill tailings% + OPC% + Fly ash%), then MI will quantify how strongly we can conclude that the specimen belongs to any specific curing period among 7, 14, 28, and 56 days; (ii) for instance, the given CPB specimens of known mix recipes have been cured for 28 days, then how much confident are we that it has acquired the critical strength ≥ 1 MPa. The results of the sensitivity analysis are explained as follows:

- The cement proportion was found to be the main contributing factor behind the strength development with a high percentage of variance reduction (57.8%) and MI (47.3%), and therefore given rank 1.
- The second most significant factor affecting the strength development inside CPB was the mill tailings proportion. This finding was in line with the previous reported studies [46, 82]. The mill tailings contribute about 33% of total variance in the paste fill strength. The oxides of calcium and magnesium in the mill tailings were observed to lie between cement and fly ash, which may have resulted in its significance next to the OPC.
- The significance of fly ash was found as next to the cement and mill tailings. The fly ash was observed to affect the strength negatively in comparison to that when replacing the cement percentage. The high specific surface area results in the finer particles coming out through the pores of the CPB, which in turn reduces the level of compaction of the CPB. The high water retention potential and low pozzolanic activity reduced the consistency and rate of solidification. As a result, the paste formed will be less stiff and of lower strength.
- The sensitivity of the curing period was found to be less than the proportion of the paste fill ingredients. The curing period shows the rate of binder hydration and formation of C-S–H gel inside paste fills which is strongly affected by the characteristics and the relative proportion of ingredients. The CPB with optimal proportion of ingredients could reduce the available pore spaces and improve the particle gradation. Therefore, the hydration products can abundantly pack the pore spaces and resulted in high dense matrix and stiff paste. These optimum proportions have been determined through joint strategies and are shown in Section 3.4.4.

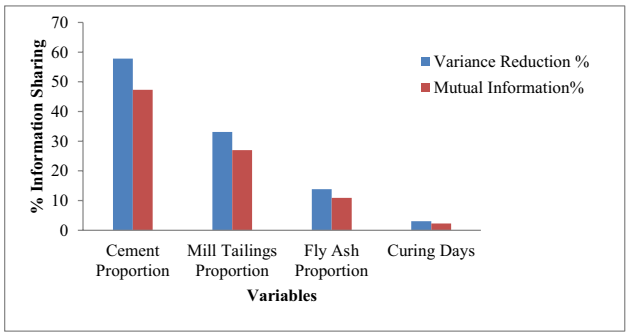

Fig. 14 Sensitivity analysis of the variables towards "strength"

3.4.4 Cross-validation of BNs

The proposed BN model was aimed to predict the CPB's strength, and it is essential to determine its validity in practical application. Before initiating the cross-validation test, it may be rather important to highlight the methodology adopted to work with the BN model. In this view, an attempt has been made to summarise the detailed steps (along with the corresponding methodology) followed from creation of the model to its validation in the form of a flowchart and presented in Fig. 15. This flowchart may be significant to develop the comprehensive understanding about the step by step procedure obligatory for classification with BN model.

To validate the BN model, a k-fold cross-validation technique is commonly employed [77]. The full dataset ($n = 96$) was equally categorised into 4 clusters, and each time, the model was trained by 3 clusters and the remaining one was used to validate the model. This process was repeated 4 times so that each dataset could be used to train and test the model to complete the fourfold cross-validation. A similar technique was also adopted by Li et al. [77] to carry out eightfold cross validation. The present developed model is also learned and validated using the whole dataset and compared with the previous reported models as shown in Table 13.

It can be seen from Table 13 that the model predicts 2 FN cases for the 1st validation group and 4 FP cases for the 2nd validation group which was the source of error in the model. Similarly for the whole datasets both FN and FP cases were obtained as the origin of error. For the fourth validation group, the model was obtained as free of any error. The values of the model

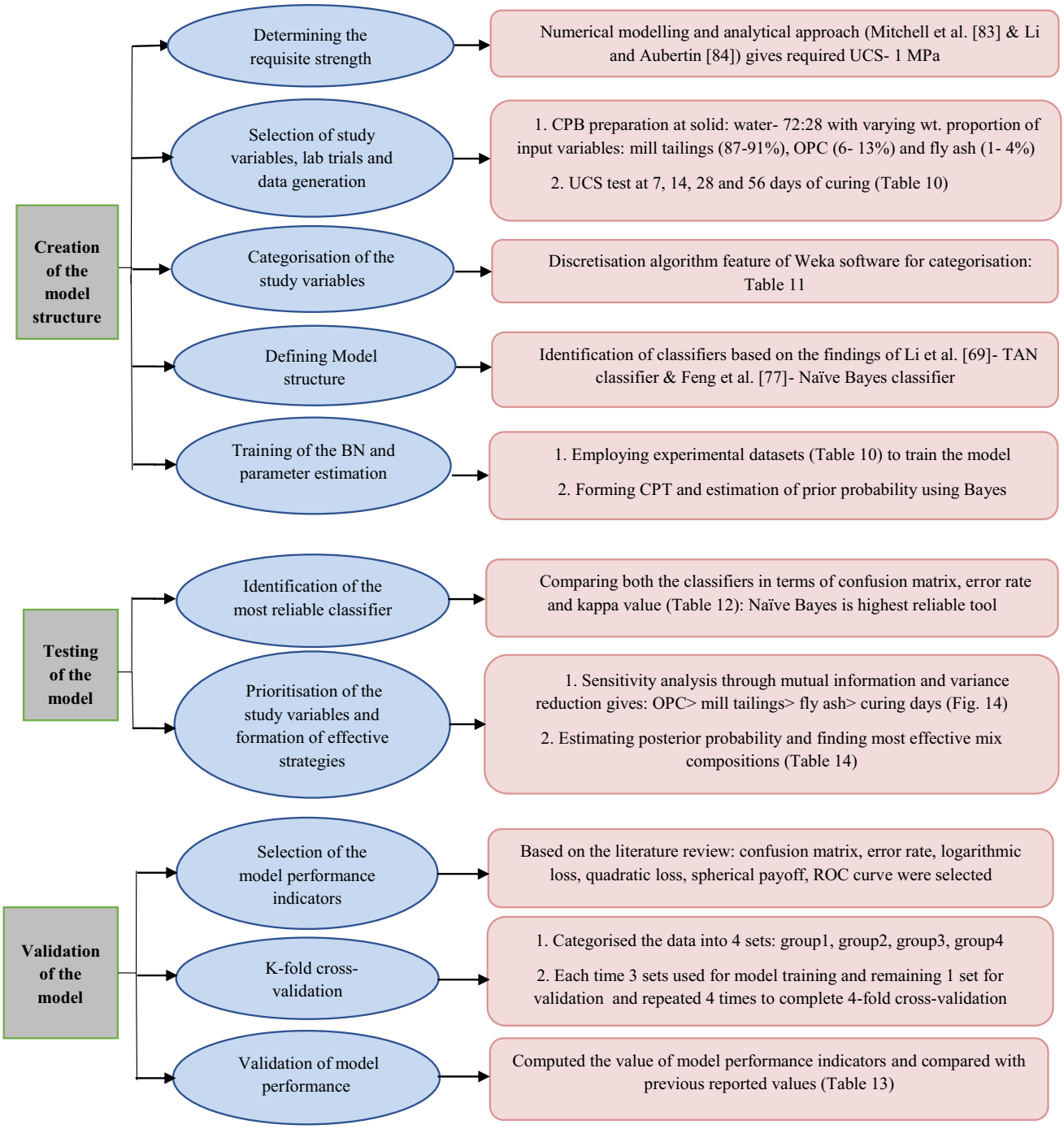

Fig. 15 Flowchart showing different steps undertaken in creation, testing, and validating the model

performance indicator (logarithmic loss, quadratic loss, spherical pay-off, and ROC curve) for the present study were also compared with that of past reported models in diverse areas. The same approach was also employed by Fam et al. [111] to check the reliability of their developed model. The comparison illustrates that the present values of these indices are in line with their corresponding reported values in the literature [111, 119, 126]. Therefore, it can be concluded that the developed model possesses good predictive ability and could be employed to characterise and optimise the strength development of the CPB within the study range of variables.

Table 13 Validity of BN model with different indicators

Validation group/reference	Error rate (%)	Logarithmic loss	Quadratic loss	Spherical pay-off	Area under ROC	Confusion matrices		
						Predicted		Actual
						Low	High	
Present study group 1	8.33	0.1597	0.079	0.9567	1	22 (TN)	0 (FP)	Low
						2 (FN)	0 (TP)	High
Present study group 2	16.67	0.2794	0.1889	0.8877	1	12 (TN)	4 (FP)	Low
						0 (FN)	8 (TP)	High
Present study group 3	12.5	0.3296	0.207	0.885	0.8492	2 (TN)	1 (FP)	Low
						2 (FN)	19 (TP)	High
Present study group 4	0	0.0376	0.0051	0.9985	1	0 (TN)	0 (FP)	Low
						0 (FN)	24 (TP)	High
Average (1–4 group)	5.21	0.2258	0.1286	0.9298	0.9878	-		
Present study (whole dataset)	9.375	0.1812	0.1094	0.9376	0.982	36 (TN)	5 (FP)	Low
						4 (FN)	51 (TP)	High
Feng and Jimenez [79]	13.35%	-	-	-	-	-		
Fam et al. [111]	15%	0.7716	0.2572	0.8513	-	-		
Korb and Nicholson [118]	9.62%	0.2562	0.1397	0.9255	0.961	-		
Kalacska et al. [141]	17.6–48.7%	0.6–1.33	0.32–0.61	0.59–0.83	-	-		

3.4.5 Joint Strategies for Optimising Strength

The joint strategy is primarily an effort to improve the probability of desired output by picking up multiple predictors at a time and allowing interaction among their states. In the context of present experimental scenario, the joint strategies will help to analyse the coupled interaction effect of the predictors on the strength and to determine the optimal mix design to acquire the desired strength after the specified curing age.

Table 14 shows the probabilistic scenario to achieve the designed strength for the control and fly ash–added specimens. The paste fill specimens prepared with 87–88% mill tailings and with 12–13% OPC can achieve the targeted strength even at 7 days of curing period. This probability varied from 99.7 to 99.8% between 7 and 56 days. Therefore, the potential of failure to the CPB structure was insignificant at 87–88% mill tailings and 12–13% OPC. The probability was slightly dropped from 99.8 to 97.1% for the paste fill specimens of $P\left(\frac{strength=high}{mill\ tailings=89-91\%,\ cement=9-11\%,\ flyash=0\%,\ curing\ days=28\ days}\right)$. For the paste fill specimens of mill tailings (87–88%)* OPC (9–11%)* fly ash (1–2%)*curing days (28 days), the probability to attain the critical strength was 98.7% and subsequently dropped to 96.8% for increasing fly ash up to 4%. The likelihood to acquire the targeted strength was 38.3% for the interaction of mill tailings (87–88%)* OPC (6–8%)* fly ash (3–4%)* curing days (28 days). For this category, only specimens prepared with 88% mill tailings, 8% OPC, and 4% fly ash surpassed the targeted strength after 28 days of curing.

Table 14 Coupled interaction effect on the strength of the paste fill specimens

Mill tailings proportion	Cement proportion	Fly ash proportion	Curing days	Prob. of high UCS
87–88%	12–13%	0%	7–14	99.7
87–88%	12–13%	0%	28	99.8
87–88%	12–13%	0%	56	99.8
89–91%	9–11%	0%	7–14	94.2
89–91%	9–11%	0%	28	97.1
89–91%	9–11%	0%	56	97.1
87–88%	9–11%	1–2%	7–14	97.4
87–88%	9–11%	1–2%	28	98.7
87–88%	9–11%	1–2%	56	98.7
87–88%	9–11%	3–4%	7–14	93.7
87–88%	9–11%	3–4%	28	96.8
87–88%	9–11%	3–4%	56	96.8
87–88%	6–8%	3–4%	7 -14	23.3
87–88%	6–8%	3–4%	28	38.3
87–88%	6–8%	3–4%	56	38.3
89–91%	9–11%	1–2%	7–14	65.9
89–91%	9–11%	1–2%	28	79.8
89–91%	9–11%	1–2%	56	79.8
89–91%	6–8%	1–2%	7–14	3.78
89–91%	6–8%	1–2%	28	7.43
89–91%	6–8%	1–2%	56	7.43
89–91%	6–8%	3–4%	7–14	1.53
89–91%	6–8%	3–4%	28	3.09
89–91%	6–8%	3–4%	56	3.09

Table 15 Result of collinearity test with correlation matrix

	Finespercentage	SSA	Slump	Bleeding	HI
Fines percentage	1	1.000	−0.224	−0.323	0.598#
SSA	1.000#	1	−0.201	−0.336	0.577#
Slump	−0.224	−0.201	1	0.624#	−0.871#
Bleeding	−0.323	−0.336	0.624#	1	−0.246
HI	0.598#	0.577#	−0.871#	−0.246	1

#Correlation is significant at the 0.01 level

The probability was found to be 79.8% for the 28 days–cured paste specimens prepared with 89–91% mill tailings, 9–11% OPC, and 1–2% fly ash. The paste fill specimens of the group $P\left(\frac{\text{strength = high}}{\text{mill tailings =days 89 − 91%, cement = 6 − 8%, fly ash = 1 − 2%, curing days = 28}}\right)$ show only 7.43% and $P\left(\frac{\text{strength = high}}{\text{mill tailings = 89 - 91%, cement = 6 - 8%, fly ash = 3 - 4%, curing days = 28 days}}\right)$ show 3.09% likelihood to attain the designed strength. The degrees of failure to the CPB structure were 92.57% and 96.91%, subsequently.

The joint strategies signify that the paste fill specimens of 87–88% mill tailings category have a high potential to attain the targeted strength with the least degree of uncertainty. The OPC could be replaced by fly ash up to 4% in the paste specimens with 87–88% mill tailings. The probability that the specimens will not achieve the targeted strength was only 3.2%. The probability to attain the targeted strength for the fly ash–mixed specimens was comparable to the specimens of control group at 87–88% mill tailings range due to a low level of uncertainties.

The likelihood of the CPB to not acquire the targeted strength varies between 20.2 and 98.47% for adding fly ash at 89–91% mill tailings proportion. It shows that the uncertainties in strength development within the specimens were significantly high at the 89–91% mill tailings range. Therefore, it can be concluded that the paste fills prepared with 87–88% mill tailings and 9–11% cement are highly reliable with the fly ash content up to 4%. The strength of CPB specimens possesses the least level of uncertainty for addition of fly ash at 87–88% mill tailings and therefore at these proportions of the ingredients the economic constraints can be reduced with due retaining the desired level of stability and safety of the CPB structure underground.

3.5 Collinearity Test

In order to address the statistical significance of the inherent characteristics of the CPB's ingredients (such as particle size distribution, chemical composition) as well as fresh CPB's properties on its strength development and to quantify the level of association between them, a collinearity test was carried out. The effect of particle size distribution was evaluated in terms of 'specific surface area' and 'fines percentage' (< 20 µm), whereas to quantify the impact of chemical composition of CPB's ingredient on its strength, hydration index (HI) was considered. The "slump" and "bleeding rate" were taken as fresh CPB's properties. Thereafter, the collinearity among the "fines percentage", "specific surface area", "slump", and "bleeding rate" was tested.

Table 16 Results of multicollinearity test

Variables	VIF
Slump	24.169
Bleeding	4.196
Fines percentage	3.691
SSA	3.542
HI	23.122

Dependent variable: UCS

There are various statistical techniques to measure the collinearity among the variables. The correlation matrix is one of the techniques that is considered here to compute the level of collinearity among the abovementioned variables [142]. The results are shown in Table 15. It can be seen that the levels of association between these variables are moderate to high. The fines proportion and SSA are both negatively correlated with the slump and bleeding rate. The correlations for the interaction "fines percentage*slump" and "fines percentage*bleeding rate" were − 0.224 and − 0.323, respectively. The findings favour the results presented in Fig. 5 (for bleeding) and Table 9 (for slump). Table 15 shows that the fines proportion and SSA of the CPB's ingredients are correlated with its hydration index at 1% statistical significance level. The correlations for the interaction groups "fines percentage*HI" and "SSA*HI were 0.598 and 0.577 at the 1% significance level. It shows that the increasing fines proportion of the CPB's ingredients significantly augments its chemical reactivity and rate of formation of hydration products. Few other correlations such as (Slump* Bleeding, Slump*HI) were also found to be statistically significant within the 1% error limit. The results of the correlation matrix show that these variables are highly correlated with each other which probably can be an indication of the presence of multicollinearity [142].

It is pertinent to mention that the correlation matrix could only measure the collinearity between a pair of factors and is not able to quantify multicollinearity. Multicollinearity is a statistical phenomenon when two or more input factors in

the regression model are highly correlated. Multicollinearity is detected by examining the value of variance inflation factor (VIF). The value of VIF < 1 shows no correlation, VIF between 1 and 5 shows a moderate level correlation, and VIF > 5 shows a high correlation [142, 143]. The values of VIF for all the input variables are summarised in Table 16. The value of VIF was quite high for the slump and HI shows the highest, thus showing a strong level of correlation with UCS. Other factors such as bleeding, fines percentage, and SSA also show a moderate level of correlation with the UCS. Based on the findings, it can be concluded that the primary characteristics of the CPB's ingredients significantly affect the fresh CPB properties and all these variables jointly correlated with the strength of the CPB.

4 Conclusion

The present study analysed the effect of fly ash as a partial substitute of the OPC on the cemented paste backfill strength. The test results indicate that the fly ash is an appropriate binding agent for partly replacing OPC in the CPB. The BN model was used to characterise the experimental data to determine the most consistent mix proportion to reduce the economic hurdles and to improve the safety of CPB's structure. Based on the significance of the study, the following conclusions can be drawn:

- The bleeding rate of fresh CPB increased with lowering OPC content in the control group of CPB because of high fines percentage of the OPC. At a fixed mill tailings proportion, replacing OPC with that of fly ash shrinks the volume of bleed water because of the high specific surface area and silica content of the fly ash. The high SSA increases the water demand of the CPB to maintain the same consistency. In addition, the high silica content densifies the CPB matrix by reducing its porosity and resulted in high water retention potential and low level of drainage. The mill tailings contain a coarser fraction than that of binders used. Therefore, the CPB prepared with 91wt% mill tailings + 9wt% cement will have a less degree of water retention capability and high drain ability than that of CPB prepared with 87wt% mill tailings + 13wt% cement. Furthermore, at a fixed mill tailings proportion, the increasing replacement level of OPC with that of fly ash will also increase the water-retaining ability of the CPB and decrease the availability of free water to drain out in the form of bleeding. The slump and spread values increased and density decreased with reducing OPC content in the control group and fly ash mixed CPB.
- The compressive strength of the control specimens decreased incessantly with escalating mill tailings proportion. It may be due to the fact that at the constant solid proportion, increasing mill tailings lessens the fraction of binder content in the paste fills. The paste specimens exhibited an inverse trend between the increasing level of fly ash addition and strength development. Most of the fly ash mixed specimens exhibited major strength variation during 14–28 days and attained their 90% strength at the curing age of 28 days. The strength development patterns within control and fly ash mixed specimens were similar but the fly ash–added specimens acquired strength at a lower rate in comparison to the specimens of control group due to a difference in binder properties.
- To model the coupled interaction effect, the BN was developed with naïve Bayes and TAN classifiers. A comparison suggests that the naïve Bayes is more reliable for modelling the paste fill strength. Through a sensitivity analysis, cement proportion was found to be highly significant towards strength growth followed by mill tailings, fly ash, and curing days.
- The joint strategies signify that with 87–88% mill tailings, the addition of fly ash resulted in the least degree of uncertainties in strength development. In this case, the maximum failure potential of the CPB structure was only 3.2%. At 89–91% mill tailings, varying fly ash content from 0 to 4% increases the likelihood of failure of the CPB structure from 2.9 to 96.91%.
- The validity of the Bayesian model is checked by means of different model performance indicators. It shows that the model can reliably capture the trend of the paste fill experimental data to decrease the economic constraints and to find out the most consistent mix proportion. The developed model will only be limited to the studied range of the predictors and required to update in case the values of the input variables are outside the testing range.
- The collinearity test between the fines percentage, SSA, HI, slump, and bleeding rate indicates that they are statistically correlated with each other as well as CPB's strength. The particle size distribution of the mix ingredients is found to strongly influence the chemical reactivity of the CPB.

The developed BN has been found to strengthen the present study by providing more insight into the experimental datasets in respect to the individual as well as coupled effect of the causal factors towards strength development of the CPB. Therefore, the predictors could be prioritised based on their relative significance and few effective mix compositions were identified. It provides a comprehensive understanding that for the given output (within the studied range), which parameter or combination of parameters preferably needs high attention.

Although the proposed naïve BN is found as an effective tool to predict the strength of the paste fill specimens, it is

not to be considered as a substitute of numerical modelling, and field trials with instrumentation and monitoring that are commonly employed to optimise the in situ efficiency of the CPB system. The performance of the model could be improved with more extensive datasets and by considering ingredients of different origins. The model could also be analysed with incorporating in situ factors like curing stress, filling rate, and stope dimension on the strength development pattern of the CPB inside stope. As it is well known fact that for the identical mix recipe, there is variation between the strength of in situ cured CPB and laboratory-cured specimens. It will be helpful in improving the in situ stability of the CPB's structure by developing more effective filling strategies.

Acknowledgements The authors would like to acknowledge Director, CSIR-CIMFR, for his constant support and guidance for completing this study.

Funding This study has been carried out with the financial support received from Hindustan Zinc Limited (HZL) and CSIR-CIMFR (MLP/81/2019–20).

Declarations

Conflict of Interest The authors declare no competing interests.

References

1. Bhattacharyya SS, Shah Y (2021) Emerging technologies in Indian mining industry: an exploratory empirical investigation regarding the adoption challenges. J Sci Technol Policy Manag. https://doi.org/10.1108/JSTPM-03-2021-0048
2. Driussi C, Jansz J (2006) Technological options for waste minimisation in the mining industry. J Clean Production 14(8):682–688
3. Wang J, Huang Z (2017) The recent technological development of intelligent mining in China. Engineering 3(4):439–444
4. Lyashenko V, Khomenko O, Golik V, Topolnij F, Helevera O (2020) Substantiation of environmental and resource-saving technologies for void filling under underground ore mining. Tech Audit Product Res 2(52):9–16. https://doi.org/10.15587/2312-8372.2020.200022
5. Yao Y, Cui Z, Wu R (2012) Development and challenges on mining backfill technology. J Mater Sci 1(4):73–78. https://doi.org/10.5539/jmsr.v1n4p73
6. Helinski M, Fahey M, Fourie A (2011) Behavior of cemented paste backfill in two mine stopes: measurements and modeling. J Geotech Geoenvironmental Eng 137(2):171–182. https://doi.org/10.1061/(ASCE)GT.1943-5606.0000418
7. Ghirian A, Fall M (2015) Coupled behavior of cemented paste backfill at early ages. Geotech Geol Eng 33:1141–1166. https://doi.org/10.1007/s10706-015-9892-6
8. Panchal S, Deb D, Sreenivas T (2018) Variability in rheology of cemented paste backfill with hydration age, binder and superplasticizer dosages. Adv Powder Technol 29(9):2211–2220. https://doi.org/10.1016/j.apt.2018.06.005
9. Yilmaz E (2017) Stope depth effect on field behaviour and performance of cemented paste backfills. Int J Min Reclam Environ 32(4):273–296. https://doi.org/10.1080/17480930.2017.1285858
10. Behera SK, Singh P, Ghosh CN, Mishra DP, Mandal PK, Verma A, Mohanty S, Mishra K, Singh PK (2019) Slump test: laboratory and numerical simulation-based approach for consistency of mill tailings paste. Curr Sci 117(2):235–241. https://doi.org/10.18520/cs/v117/i2/235-241
11. Belem T, Benzaazoua M (2008) Design and application of underground mine paste backfill technology. Geotech Geol Eng 26:147–174. https://doi.org/10.1007/s10706-007-9167-y
12. Zheng J, Tang Y, Feng H (2021) Utilization of low-alkalinity binders in cemented paste backfill from sulphide-rich mine tailings. Constr Build Mater 290:123221. https://doi.org/10.1016/j.conbuildmat.2021.123221
13. Sveinson S (1999) Characterisation of tailings for paste backfill system design. Dissertation, University of British Columbia. https://open.library.ubc.ca/collections/ubctheses/831/items/1.0081175. Accessed 13 July 2022
14. Henderson A, Revell MB, Landriault D, Coxon J (2005) Paste fill. In: Potvin Y, Thomas E, Fourie A (eds) Handbook on mine fill, Australian Center for Geomechanics, Perth, pp 83–97
15. Hasan, A, Suazo, G, Doherty, JP & Fourie, AB (2014) In situ measurements of cemented paste backfilling in an operating stope at Lanfranchi Mine. In: Y Potvin & T Grice (eds), Mine Fill, Proceedings of the Eleventh International Symposium on Mining with Backfill, Australian Centre for Geomechanics, Perth, pp. 327–336. https://doi.org/10.36487/ACG_rep/1404_26_Hasan
16. Kesimal A, Ercikdi B, Yilmaz E (2003) The effect of desliming by sedimentation on paste backfill performance. Miner Eng 16(10):1009–1011. https://doi.org/10.1016/S0892-6875(03)00267-X
17. Fall M, Benzaazoua M, Ouellet S (2005) Experimental characterization of the influence of tailings fineness and density on the quality of cemented paste backfill. Miner Eng 18(1):41–44. https://doi.org/10.1016/j.mineng.2004.05.012
18. Huang S, Xia K, Qiao L (2011) Dynamic tests of cemented paste backfill: effects of strain rate, curing time, and cement content on compressive strength. J Mater Sci 46(15):5165–5170. https://doi.org/10.1007/s10853-011-5449-0
19. Singh P, Ghosh CN, Behera SK, Mishra K, Kumar D, Buragohain J, Mandal PK (2019) Optimisation of binder alternative for cemented paste fill in underground metal mines. Arab J Geosci 12:462. https://doi.org/10.1007/s12517-019-4623-6
20. Rankine RM, Rankine KJ, Sivakugan N, Karunasena W, Bloss ML (2001a) Geotechnical characterization and stability analysis of BHP Cannington paste backfill. In: Proceedings of the 15th international conference on soil mechanics and geotechnical engineering, pp 1241–1244. https://www.researchgate.net/publication/237739917_Geotechnical_Characterisation_and_Stability_Analysis_of_BHP_Cannington_Paste_Backfill. Accessed 13 July 2022
21. Célestin JCH, Fall M (2009) Thermal conductivity of cemented paste backfill material and factors affecting it. IJMRE 23(4):274–290. https://doi.org/10.1080/17480930902731943
22. Fall M, Benzaazoua M (2005) Modeling the effect of sulphate on strength development of paste backfill and binder mixtures optimization. Cem Concr Res 35(2):301–314. https://doi.org/10.1016/j.cemconres.2004.05.020
23. Fall M, Benzaazoua M, Saa EG (2008) Mix proportioning of underground cemented tailings backfill. Tunn Under Sp Tech 23(1):80–90. https://doi.org/10.1016/j.tust.2006.08.005
24. Belem T, Fourie AB, Fahey M (2010) Time-dependent failure criterion for cemented paste backfills. In: Proceeding of the 13th International Seminar on Paste and Thickened Tailings. Australian Centre for Geomechanics, Canada, pp 147–162. https://doi.org/10.36487/ACG_rep/1063_13_Belem

25. Kang D, Seo KS, Lee HY, Chung W (2017) Experimental study on mechanical strength of GO-cement composites. Constr Build Mater 131:303–308. https://doi.org/10.1016/j.conbuildmat.2016.11.083
26. Fall M, Pokharel M (2010) Coupled effects of sulphate and temperature on the strength development of cemented tailings backfills: Portland cement-paste backfill. Cem Concr Comp 32(10):819–828. https://doi.org/10.1016/j.cemconcomp.2010.08.002
27. Chen QS, Zhang QL, Fourie A, Chen X, Qi C (2017) Experimental investigation on the strength characteristics of cement backfill in a similar stope model and its mechanism. Constr Build Mater 154:34–43. https://doi.org/10.1016/j.conbuildmat.2017.07.142
28. Qiu Y, Sego DC (2001) Laboratory properties of mine tailings. Can Geotech J 38(1):183–190. https://doi.org/10.7939/R3WW7704C
29. Yilmaz E, Kesimal A, Ercikti B, Ail I (2003) Determination of optimum cements content for paste backfill samples. In: Proceeding18th International Mining Congress and Exhibition of Turkey-IMCET 2003, ro 2003, Antalya, Turkey, pp 119–125
30. Benzaazoua M, Fall M, Belem T (2004) A contribution to understanding the hardening process of cemented paste fill. Miner Eng 17:141–152. https://doi.org/10.1016/j.mineng.2003.10.022
31. Abdellah WR, Ali MA (2017) Stability analysis of vertical and inclined backfilled stope. J Eng Sci 45(1):70–79. https://doi.org/10.21608/jesaun.2017.116089
32. Behera SK, Ghosh CN, Mishra DP, Singh P, Mishra K, Buragohain L, Mandal PK (2020) Strength development and microstructural investigation of lead-zinc mill tailings based paste backfill with a fly ash as alternate binder. Cem Concr Res 109:103553. https://doi.org/10.1016/j.cemconcomp.2020.103553
33. Landriault D (1995) Paste backfill mix design for Canadian underground hard rock mining. In: Proceedings of the 97th annual general meeting of the CIM rock mechanics and strata control session, Canadian institute of mining, metallurgy and petroleum, Halifax, NS, Canada, pp 229–238
34. Grice T (1998) Underground mining with backfill. In: proceeding 2nd Annual Summit on Mine Tailings Disposal Systems, Brisbane, Australia. https://www.academia.edu/41792455/Underground_Mining_with_Backfill. Accessed 13 July 2022
35. Yumlu M (2001) Backfill practices at Cayeli Mine. In: Proceedings of the 17th International Mining Congress and Exhibition of Turkey, E.Unal (ed.), Kozan Publisher, Ankara, pp 333–339
36. Been K, Brown ET, Hepworth N (2002) Liquefaction potential of paste fill at Neves Corvo Mine. Portugal IMM Transact Sect A 111(1):47–58. https://doi.org/10.1179/mnt.2002.111.1.47
37. Roux LK, Bawden WF, Grabinsky MW (2004) 'Liquefaction analysis of early age cemented paste backfill. In: Proceedings of the 8th International Symposium on Mining with Backfill (MineFill 2004), The Nonferrous Metals Society of China, Beijing, pp. 233–241
38. Fall M, Benzaazoua M (2003) Advances in predicting performance properties and cost of paste backfill. Proceedings on tailings and mine waste'03. Vail, USA, pp 73–85
39. Klein K, Simon D (2006) Effect of specimen composition on the strength development in cemented paste backfill. Canad Geotech J 43:310–324. https://doi.org/10.1139/t06-005
40. Fall M, Celestin JC, Pokharel M, Toure M (2010) A contribution to understanding the effects of curing temperature on the mechanical properties of mine cemented tailings backfill. Eng Geol 114:397–413. https://doi.org/10.1016/j.enggeo.2010.05.016
41. Cihangir F, Erçıkdı B, Turan A, Kesimal A, Deveci H, Yazıcı M and Karaoğlu K (2011) Utilisation of sodium silicate activated blast furnace slag as an alternative binder in paste backfill of high-sulphide mill tailings, in, Paste 2011: Proceedings of the 14th international seminar on paste and thickened tailings, R Jewell & AB Fourie (eds), Australian Centre for Geomechanics, Perth, pp. 465–475. https://doi.org/10.36487/ACG_rep/1104_40_Cihangir
42. Cihangir F, Ercikdi B, Kesimal A, Turan A, Deveci H (2012) Utilisation of alkali-activated blast furnace slag in paste backfill of high-sulphide mill tailings: effect of binder type and dosage. Miner Eng 30:33–43. https://doi.org/10.1016/j.mineng.2012.01.009
43. Cihangir F, Ercikdi B, Kesimal A, Deveci H, Erdemir F (2015) Paste backfill of high-sulphide mill tailings using alkali-activated blast furnace slag: effect of activator nature, concentration and slag properties. Miner Eng 83:117–127. https://doi.org/10.1016/j.mineng.2015.08.022
44. Bernier RL, Lee MG, Moerman A (1999) Effects of tailings and binder geochemistry on the physical strength of paste backfill. In: Proceedings of Sudbury '99, Mining and the environment II, Sudbury, Canada, pp 1113–1122. https://pdf.library.laurentian.ca/medb/conf/Sudbury99/NewTech/NTOP8.PDF. Accessed 13 July 2022
45. Ouellet J, Benzaazoua M, Servant S (1998) Mechanical, mineralogical and chemical characterization of a paste backfill. In: Proceedings of Tailings and Mine Waste'98 (5 ; Fort Collins 1998-01-26), Colorado, A.A. Balkema, Rotterdam, pp 139–146. https://pascal-francis.inist.fr/vibad/index.php?action=getRecordDetail&idt=6214630. Accessed 13 July 2022
46. Benzaazoua M, Ouellet J, Servant S, Newman P, Verburg R (1999) Cementitious backfill with high sulphur content: physical, chemical and mineralogical characterization. Cem Concr Res 29:719–725. https://doi.org/10.1016/S0008-8846(99)00023-X
47. Li L, Aubertin M (2009) A three-dimensional analysis of the total and effective normal stresses in submerged backfilled stopes. Geotech Geol Eng 27(4):559–569. https://doi.org/10.1007/s10706-009-9257-0
48. Hughes P, Pakalnis RT, Caceres C, Blake W, Brady TM (2006) Numerical modeling of paste sills in underhand cut & fill stopes. Third International Seminar on Deep and High Stress Mining, Quebec City, Quebec. Universite Laval, Canada, pp 1–10
49. Liu Q, Liu DF, Tian Y, Liu X (2017) Numerical simulation of stress-strain behaviour of cemented paste backfill in triaxial compression. Eng Geol 231:165–175. https://doi.org/10.1016/j.enggeo.2017.10.021
50. Newman, Christopher Richard (2018) Numerical analysis of stress distributions for multiple backfilled stopes. Dissertations, p 43. https://uknowledge.uky.edu/mng_etds/43; https://doi.org/10.13023/etd.2018.302
51. Veenstra RL, Bawden WF, Grabinsky MW Thompson BD (2007) An approach to stope scale numerical modelling of early age cemented paste backfill. In: Proceedings of 45th U.S. Rock Mechanics/ Geomechanics Symposium, San Francisco, California, Paper Number: ARMA-11-274. https://doi.org/10.1061/(ASCE)1090-0241133:10(1308)
52. Wu D, Fall M, Cai S (2014) Numerical modelling of thermally and hydraulically coupled processes in hydrating cemented tailings backfill columns. IJMRE 28:173–199. https://doi.org/10.1080/17480930.2013.809194
53. Rankine RM, Rankine KJ, Sivakugan N, Karunasena W, Bloss ML (2001) A numerical analysis of the arching mechanism in paste fill during a complete mining sequence. Computational Mechanics–New Frontiers for the New Millennium, pp 461–466. https://doi.org/10.1016/B978-0-08-043981-5.50071-7
54. Rankine RM, Sivakugan N (2006) Prediction of paste backfill performance using artificial neural networks. In: Proceedings of the 16th International Conference on Soil Mechanics and

Geotechnical Engineering, pp. 1107–1110. https://doi.org/10.3233/978-1-61499-656-9-1107
55. Qi C, Fourie A, Chen Q, Zhang Q (2018) A strength prediction model using artificial intelligence for recycling waste tailings as cemented paste backfill. J Clean Prod 183:566–578. https://doi.org/10.1016/j.jclepro.2018.02.154
56. Qi C, Chen Q, Fourie A, Zhang Q (2018) An intelligent modelling framework for mechanical properties of cemented paste backfill. Miner Eng 123:16–27. https://doi.org/10.1016/j.mineng.2018.04.010
57. Qi C, Chen Q, Fourie A, Tang X, Zhang Q, Dong X, Feng Y (2019) Constitutive modelling of cemented paste backfill: a data-mining approach. Constr Build Mater 197:262–270. https://doi.org/10.1016/j.conbuildmat.2018.11.142
58. Benzaazoua M, Belem T, Bruno B (2002) Chemical factors that influence the performance of mine sulphidic paste backfill. Cem Concr Res 32:1133–1144. https://doi.org/10.1016/S0008-8846(02)00752-4
59. Yilmaz E, Belem T, Bussière B, Benzaazoua M (2008) Consolidation characteristics of early age cemented paste backfill. GeoEdmonton 797–804. https://www.researchgate.net/publication/237817708_Consolidation_characteristics_of_early_age_cemented_paste_backfill. Accessed 13 July 2022
60. Kesimal A, Yilmaz E, Ercikdi B, Alp I, Deveci H (2005) Effect of properties of tailings and binder on the short-and long-term strength and stability of cemented paste backfill. Mater Lett 59:3703–3709. https://doi.org/10.1016/j.matlet.2005.06.042
61. Hane, I, Belem, T, Benzaazoua, M and Maqsoud, A (2017) Laboratory investigation into the compressive strength of cemented paste tailings aggregate fills', In: M Hudyma & Y Potvin (eds), UMT 2017: Proceedings of the first international conference on underground mining technology, Australian Centre for Geomechanics, Perth, pp. 363–373. https://doi.org/10.36487/ACG_rep/1710_28_Hane
62. Zhang X, Lin J, Liu J, Li F, Pang Z (2017) Investigation of hydraulic-mechanical properties of paste backfill containing coal gangue-fly ash and its application in an underground coal mine. Energies 10(9):1309. https://doi.org/10.3390/en10091309
63. Hassani F, Ouellet J, Servant S (2001) In situ measurements in a paste backfill: backfill and rock mass response in the context of rockburst. In: proceedings of 17th international mining congress and exhibition of Turkey (IMCET2001), pp 165–175. https://www.maden.org.tr/resimler/ekler/d38dd921e155207_ek.pdf. Accessed 13 July 2022
64. Thompson BD, Grabinsky MW, Bawden WF, Counter DB (2009) In-situ measurements of cemented paste backfill in long-hole stopes. Proceedings of the 3rd Canada-US Rock Mechanics Symposium & 20th Canadian Rock Mechanics Symposium, in M Diederichs & G Grasselli (eds), University of Toronto Press, Toronto, on CD-ROM. https://www.researchgate.net/publication/309900380_In-situ_measurements_of_cemented_paste_backfill_in_long-hole_stopes. Accessed 13 July 2022
65. Hasan A, Suazo G, Doherty JP, Fourie AB (2014) In situ measurements of cemented paste backfilling in an operating stope at Lanfranchi Mine. In: Proceedings of Eleventh International Symposium on Mining with Backfill (Mine Fill 2014), Australian Centre for Geomechanics, Perth, pp 327–336. https://papers.acg.uwa.edu.au/p/1404_26_Hasan/
66. Grabinsky M, Thompson BD, Bawden WF (2011) In-situ measurements of paste backfill pressure in a narrow, dipping stope. In: Proceedings of 14th Pan-American Conference on Soil Mechanics and Geotechnical Engineering 64th Canadian Geotechnical Conference, Toronto, Ontario, Canada
67. Orejarena L, Fall M (2010) Artificial neural network based modeling of the coupled effect of sulphate and temperature on the strength of cemented paste backfill. Can J Civ Eng 38(1):100–109. https://doi.org/10.1139/L10-109
68. Deng X, Zhang J, Tao K, Wang D (n.d.) Application of BP neural network in predicting the cement materials performance. J Chem Pharm Res 6(6):1681–1688. https://www.researchgate.net/publication/288209062_Application_of_BP_neural_network_in_predicting_the_cement_materials_performance. Accessed 13 July 2022
69. Cui L, Fall M (2015) A coupled thermo–hydro-mechanical–chemical model for underground cemented tailings backfill. Tunn Undergr Space Technol 50:396–414. https://doi.org/10.1016/j.tust.2015.08.014
70. Cui L, Fall M (2016) An evolutive elasto-plastic model for cemented paste backfill. Comput Geotech 71:19–29. https://doi.org/10.1016/j.compgeo.2015.08.013
71. Wu D, Deng T, Zhao R (2018) A coupled THMC modelling application of cemented coal gangue-fly ash backfill. Constr Build Mater 158:326–336. https://doi.org/10.1016/j.conbuildmat.2017.10.009
72. Permai SD, Tanty H (2018) Linear regression model using Bayesian approach for energy performance of residential building. Procedia Comput Sci 135:671–677. https://doi.org/10.1016/j.procs.2018.08.219
73. Kiureghiana AD, Ditlevsen O (2009) Aleatory or epistemic? Does it matter? Struct Saf 31(2):105–112. https://doi.org/10.1016/j.strusafe.2008.06.020
74. Kulhawy FH (1996) From Casagrande's 'calculated risk' to reliability-based design in foundation engineering. Civ Eng Pract 11:43–56
75. Christian JT (2004) Geotechnical engineering reliability: how well do we know what we are doing? J Geotech Geoenviron 130:985–1003. https://doi.org/10.1061/(ASCE)1090-0241(2004)130:10(985)
76. Kim YG, Lee SM, Seong PH (2017) A methodology for a quantitative assessment of safety culture in NPPs based on Bayesian networks. Ann Nucl Energy 102:23–36. https://doi.org/10.1016/j.anucene.2016.08.023
77. Li N, Jimenez R, Feng X (2017) The influence of Bayesian networks structure on rock burst hazard prediction with incomplete data. Procedia Eng 191:206–214. https://doi.org/10.1016/j.proeng.2017.05.173
78. Wang Y, Cao Z, Li D (2016) Bayesian perspective on geotechnical variability and site characterization. Eng Geol 203:117–125. https://doi.org/10.1016/j.enggeo.2015.08.017
79. Feng X, Jimenez R (2015) Predicting tunnel squeezing with incomplete data using Bayesian networks. Eng Geol 195:214–224. https://doi.org/10.1016/j.enggeo.2015.06.017
80. Wang Y, Cao Z (2013) Probabilistic characterization of Young's modulus of soil using equivalent samples. Eng Geol 159:106–118. https://doi.org/10.1016/j.enggeo.2013.03.01
81. Cao Z, Wang Y (2014) Bayesian model comparison and selection of spatial correlation functions for soil parameters. Struct Saf 49:10–17. https://doi.org/10.1016/j.strusafe.2013.06.003
82. Norsys Software Corporation (1998) Netica application user's guide. Norsys Software Corporation, Vancouver, BC, 1998 Canada. https://norsys.com/download.html
83. Mitchel RJ, Olsen RS, Smith JD (1982) Model studies on cemented tailings used in mine backfilling. Can Geotech J 19:14–28. https://doi.org/10.1139/t82-002
84. Li L, Aubertin MA (2012) A modified solution to assess the required strength of exposed backfill in mine stopes. Can Geotech J 49:994–1002. https://doi.org/10.1139/t2012-056
85. Landriault D, Verburg R, Cincilla W, Welch D (1997) Paste technology for underground backfill and surface tailings disposal applications. In: Short Course notes – in Canadian

Institute of Mining and Metallurgy Technical Workshop, Westmount, p 120
86. Fall M, Célestin JC, Pokharel M, Touré M (2010) A contribution to understanding the effects of curing temperature on the mechanical properties of mine cemented tailings backfill. Eng Geol 114:397–413. https://doi.org/10.1016/j.enggeo.2010.05.016
87. Ercikdi B, Cihangir F, Kesimal A, Deveci H (2017) Practical Importance of Tailings for Cemented Paste Backfill. In: Yilmaz, E., Fall, M. (eds) Paste Tailings Management. Springer, Cham. https://doi.org/10.1007/978-3-319-39682-8_2
88. Kesimal A, Yılmaz E, Ercikdi B (2004) Evaluation of paste backfill test results obtained from different size slumps with varying cement contents for sulphur rich mill tailings. Cem Concr Res 34:1817–1822. https://doi.org/10.1016/j.cemconres.2004.01.018
89. Tariq A, Nehdi M (2007) Developing durable paste backfill from sulphidic tailings. Waste Res Manage 160(4):155–166. https://doi.org/10.1680/warm.2007.160.4.155
90. Ercikdi B, Cihangir F, Kesimal A, Deveci H, Alp İ (2009) Utilization of industrial waste products as pozzolanic material in cemented paste backfill of high sulphide mill tailings. J Hazard Mater 168(2–3):848–856. https://doi.org/10.1016/j.jhazmat.2009.02.100
91. Ercikdi B, Cihangir F, Kesimal A, Deveci H, Alp İ (2010) Utilization of water-reducing admixtures in cemented paste backfill of sulphide-rich mill tailings. J Hazard Mater 179:940–946. https://doi.org/10.1016/j.jhazmat.2010.03.096
92. Landriault D (2001) Backfill in underground mining. In: Hustrulid WA (ed) Underground mining methods engineering fundamentals and international case studies. SME, New York, pp 608–609
93. Ercikdi B, Baki H, Izki M (2013) Effect of desliming of sulphide-rich mill tailings on the long-term strength of cemented paste backfill. J Environ Manage 115:5–13. https://doi.org/10.1016/j.jenvman.2012.11.014
94. Cihangir F, Akyol Y (2020) Effect of desliming of tailings on the fresh and hardened properties of paste backfill made from alkali-activated slag. Adv Mater Sci Eng. https://doi.org/10.1155/2020/4536257
95. Bella G (2021) Water retention behaviour of tailings in unsaturated conditions. Geomech Eng 26(2):117–132. https://doi.org/10.12989/gae.2021.26.2.117
96. Hassani F, Archibald J (1998) Mine backfill. Canadian Institute of Mine, Metallurgy and Petroleum (CD-ROM), Canada
97. Yin S, Shao Y, Wu A, Rao Y, Chen X (2017) Deformation behaviours of cemented backfill using sulphide-content tailings In: Proceedings of 20th International Seminar on Paste and Thickened Tailings, A Wu & R Jewell (eds), Paste, University of Science and Technology Beijing, Beijing, China, pp 315–327. https://doi.org/10.36487/ACG_rep/1752_35_Yin
98. Qui J, Yang L, Sun X, Xing J, Li S (2017) Strength characteristics and failure mechanism of cemented super-fine unclassified tailings backfill. Miner 7:58. https://doi.org/10.3390/min7040058
99. Dong Q, Liang B, Jia L, Jiang L (2019) Effect of sulfide on the long-term strength of lead-zinc tailings cemented paste backfill. Constr Build Mater 200:436–446. https://doi.org/10.1016/j.conbuildmat.2018.12.069
100. Ercikdi B, Kesimal A, Cihangir F, Deveci H, Alp İ (2009) Cemented paste backfill of sulphide-rich tailings: importance of binder type and dosage. Cement Concrete Comp 31(4):268–274. https://doi.org/10.1016/j.cemconcomp.2009.01.008
101. Ercikdi B, Külekci G, Yılmaz T (2015) Utilization of granulated marble wastes and waste bricks as mineral admixture in cemented paste backfill of sulphide-rich tailings. Construct Build Mater 93:573–583. https://doi.org/10.1016/j.conbuildmat.2015.06.042
102. Behera SK, Ghosh CN, Mishra K, Mishra DP, Singh P, Mandal PK, Buragohain J, Sethi MK (2020) Utilisation of lead–zinc mill tailings and slag as paste backfill materials. Environ Earth Sci 79(16):389. https://doi.org/10.1007/s12665-020-09132-x
103. Ye H, Gao X, Wanga R, Wang H (2017) Relationship among particle characteristic, water film thickness and flowability of fresh paste containing different mineral admixtures. Constr Build Mater 153:193–201. https://doi.org/10.1016/j.conbuildmat.2017.07.093
104. Moghaddam F, Sirivivatnanon V, Vessalas K (2018) The effect of fly ash fineness on heat of hydration, microstructure, flow and compressive strength of blended cement pastes. Case Stud Constr Mater. https://doi.org/10.1016/j.cscm.2019.e00218
105. Sevim Ö, Demir I (2019) Optimization of fly ash particle size distribution for cementitious systems with high compactness. Constr Build Mater 195:104–114. https://doi.org/10.1016/j.conbuildmat.2018.11.080
106. ASTM C39 / C39 M-20 (1996) Standard test method for compressive strength of cylindrical concrete specimens. ASTM International. https://www.file://C:/Users/Dr.%20C.N.%20Ghosh/Downloads/idoc.pub_astm-c39-c39m-standard-test-method-for-compressive-strength-of-cylindrical-concrete-specimenspdf.pdf. Accessed 13 July 2022
107. ASTM C143 / C143M - 15a (2015) Standard test method for slump of hydraulic-cement concrete, ASTM International. https://idoc.pub/documents/astm-c143-slump-testpdf-d4pqv57ox6np. Accessed 13 July 2022
108. ASTM C232/C232M: Standard Test Method for Bleeding of Concrete. https://idoc.pub/documents/standard-test-methods-for-bleeding-of-concrete-astm-c232-c232m-9n0k7yx29p4v. Accessed 13 July 2022
109. Neapolitan RE (2004) Learning Bayesian networks. Prentice Hall, Upper Saddle River, New Jersey
110. Jensen FV, Nielsen TD (2009) Bayesian networks and decision graphs. Springer Science & Business Media, New York
111. Fam IM, Ghasemi F, Kalatpour O, Moghimbeigi A (2017) Constructing a Bayesian network model for improving safety behavior of employees at workplaces. Appl Ergon 58:35–47. https://doi.org/10.1016/j.apergo.2016.05.006
112. García-Herrero S, Mariscal M, Gutierrez JM, Toca-Otero A (2013) Bayesian network analysis of safety culture and organizational culture in a nuclear power plant. Saf Sci 53:82–95. https://doi.org/10.1016/j.ssci.2012.09.004
113. García-Herrero S, Mariscal MA, Gutierrez JM, Ritzel DO (2013) Using Bayesian networks to analyze occupational stress caused by work demands: preventing stress through social support. Accid Anal Prev 57:114–123. https://doi.org/10.1016/j.aap.2013.04.009
114. Leu SS, Chang CM (2013) Bayesian-network-based safety risk assessment for steel construction projects. Accid Anal Prev 54:122–133. https://doi.org/10.1016/j.aap.2013.02.019
115. Zhao L, Wang X, Qian Y (2012) Analysis of factors that influence hazardous material transportation accidents based on Bayesian networks: a case study in China. Saf Sci 50:1049–1055. https://doi.org/10.1016/j.ssci.2011.12.003
116. Rivas T, Matías JM, Taboada J, Argüelles A (2007) Application of Bayesian networks to the evaluation of roofing slate quality. Eng Geol 94:27–37. https://doi.org/10.1016/j.enggeo.2007.06.002
117. Dempster AP, Laird NM, Rubin DB (1977) Maximum likelihood from incomplete data via EM algorithm. JR Sat Soc B Methodology 39:1–38

118. Korb KB, Nicholson AE (2010) Bayesian artificial intelligence. CRC Press
119. Dlamini WM (2010) A Bayesian belief network analysis of factors influencing wildfire occurrence in Swaziland. Environ Model Softw 25:199–208. https://doi.org/10.1016/j.envsoft.2009.08.002
120. Morgan MG, Henrion M (1990) Uncertainty: a guide to dealing with uncertainty in quantitative risk and policy analysis. Cambridge Press, New York
121. Marcot BG, Douglas Steventon J, Glenn DS, Robert KM (2006) Guidelines for developing and updating Bayesian belief networks applied to ecological modelling and conservation. Can J For Res 36:3063–3074. https://doi.org/10.1139/X06-135
122. Cohen J (1960) A coefficient of agreement for nominal scales. Educ Psych Measurement 20:37–46. https://doi.org/10.1177/001316446002000104
123. Landis JR, Koch GG (1979) The measurement of observer agreement for categorical data. Biometrics 33:159–174
124. Donker DK, Hasman A, Van GHP (1993) Interpretation of low kappa values. Int J Biomed Comput 33:55–64
125. Colwell RG, Dawid AP, Speigelhalter DJ (1993) Sequential model criticism in probabilistic expert systems. IEEE Trans Pattern Anal Mach Intell 15(3):209–219. https://doi.org/10.1109/34.204903
126. Korb KB, Nicholson AE (2004) Bayesian artificial intelligence. Chapman and Hall/ CRC Press, London
127. Fielding AH, Bell JF (1997) A review of methods for the assessment of prediction errors in conservation presence/absence models. Environ Conserv 24:38–49. https://doi.org/10.1017/S0376892997000088
128. Pepe MS, Cai T, Longton G (2006) Combining predictors for classification using the area under the receiver operating characteristic curve. Biometrics 62(1):221–229. https://doi.org/10.1111/j.1541-0420.2005.00420.x
129. Cumming GS (2000) Using between-model comparisons to FINE tune linear models of species ranges. J Biogeogr 27:441–455. https://doi.org/10.1046/j.1365-2699.2000.00408.x
130. Rice ME, Harris GT (2005) Comparing effect sizes in follow-up studies: ROC area, Cohen's d, and r. Law Hum Behav 29(5):615–620. https://doi.org/10.1007/s10979-005-6832-7
131. Gibson LA, Wilson BA, Aberton JG (2004) Landscape characteristics associated with species richness and occurrence of small native mammals inhabiting a coastal heathland: a spatial modeling approach. Biol Conserv 120:75–89. https://doi.org/10.1016/j.biocon.2004.01.027
132. Hessl A, Miller J, Kernan J, Keenum D, McKenzie D (2007) Mapping paleo wildfire boundaries from binary point data: comparing interpolation methods. Prof Geogr 59(1):87–104. https://doi.org/10.1111/j.1467-9272.2007.00593.x
133. Pearl J (1991) Probabilistic reasoning in intelligent systems: networks of plausible inference, 2nd edn. Morgan Kaufmann, San Mateo, CA
134. Pearl J (1998) Probabilistic reasoning in intelligent systems: networks of plausible inference. Morgan Kaufmann, San Mateo, California
135. Pollino CA, Woodberry O, Nicholson A, Korb K, Hart BT (2007) Parameterisation and evaluation of a Bayesian belief network for use in an ecological risk assessment. Environ Model Softw 22(8):1140–1152. https://doi.org/10.1016/j.envsoft.2006.03.006
136. Nieminen P, Seppanen P (1983) The use of blast-furnace slag and other by-products as binding agents in consolidated backfilling at Outokumpu Oy's mines. In: Granholm S (ed) Mining with backfill. Lulea University of Technology, Sweden, pp 49–58
137. Paya MEPJ, Monzó J (1993) Influence of different sized fractions of a fly ash on workability of mortars. Cem Concr Res 23(4):917–924. https://doi.org/10.1016/0008-8846(93)90045-B
138. Ferraris CF, Obla KH, Hill R (2001) The influence of mineral admixtures on the rheology of cement paste and concrete. Cem Concr Res 31(2):245–255. https://doi.org/10.1016/S0008-8846(00)00454-3
139. Patel BG, Desai A K, Shah S G (2015) Effect of binder volume on fresh and harden properties of self compacting concrete. IJERT 4(9). https://doi.org/10.17577/IJERTV4IS090628
140. Hall M, Frank E, Holmes G, Pfahringer B, Reutemann P, Witten IH (2009) The WEKA data mining software: an update. SIGKDD Explor 11(1):10–18
141. Kalacska M, Sanchez-Azofeifa G, Caelli T, Rivard B, Boerlage B (2005) Estimating leaf area index from satellite imagery using Bayesian networks. IEEE Trans Geosci Remote Sens 43:1866–1873. https://doi.org/10.1109/TGRS.2005.848412
142. Daoud J I (2017) Multicollinearity and regression analysis. In Proc: IOP Conf. Series: Journal of Physics Conf. Series, 949**,** 012009. https://doi.org/10.1088/1742-6596/949/1/012009
143. Jensen DR, Ramirez DE (2012) Variance inflation in regression. Adv Decis Sci 2013:1–15. https://doi.org/10.1155/2013/671204